Fractional Wannier Orbitals and Tight-Binding Gauge Fields in Kitaev Honeycomb Superlattices with Flat Majorana Bands

K. B. Yogendra,[1] G. Baskaran,[2,3,4] and Tanmoy Das[1]

[1]*Department of Physics, Indian Institute of Science, Bangalore 560012, India*
[2]*The Institute of Mathematical Sciences, CIT Campus, Chennai 600 113, India*
[3]*Department of Physics, Indian Institute of Technology Madras, Chennai 600036, India*
[4]*Perimeter Institute for Theoretical Physics, Waterloo, Ontario N2L 2Y5, Canada*

(Received 6 August 2024; revised 8 February 2025; accepted 12 May 2025; published 17 July 2025)

Fractional excitations hold immense promise for both fundamental physics and quantum technologies. However, constructing lattice models for their dynamics under gauge fields remains a formidable challenge due to inherent obstructions. Here, we introduce a novel and systematic framework for deriving low-energy lattice models of fractional orbitals coupled to tight-binding gauge fields. Departing from conventional geometric approaches, our method systematically eliminates the high-energy states via virtual hopping, thereby deriving the gauge potential and quantum metric through a superexchange mechanism. We demonstrate the framework by constructing Wannier orbitals for Majorana states and a tight-binding Z_2 gauge field across various flux-crystalline phases in the Kitaev spin model on a honeycomb lattice. Our study reveals a striking phase transition between two nontrivial topological phases characterized by gapless flat band with extensive degeneracy. Furthermore, we develop a gauge-invariant mean-field theory for interacting Majorana orbitals, leading to a fractional Chern state. Our work establishes a general framework for gauge-mediated tight-binding models and a gauge-invariant mean-field theory for interacting fractional orbitals that can be readily extended to U(1), SU(N) lattice gauge theories.

DOI: 10.1103/37kh-kc81

Subject Areas: Condensed Matter Physics, Strongly Correlated Materials, Topological Insulators

I. INTRODUCTION

The key to harnessing quantum materials for quantum technologies lies in engineering and controlling emergent excitations that obey unique statistics [1–7]. The sought-after excitations such as spinon, anyon, Majorana, and parafermion live on the enlarged states embedded in physical many-body Hilbert space of electrons or quantum spins. In the effective field theories for these emergent excitations, the influence of the remaining degrees of freedom is incorporated through a geometric term [8–15]. This couples the matter excitations with the emergent gauge fields to commence exotic statistics that enjoy constrained, protected, and slow dynamics of various characteristics [16–19].

Understanding the local wave function properties of emergent fractional particles is crucial for their detection and manipulation. Computations of matrix elements, selection rules, and the linear or nonlinear response to *local* probe fields [20–22] rely critically on the symmetry and localization of the Wannier orbital wave function. For this purpose, a systematic derivation of effective low-energy lattice models for fractional particles is essential.

Within a lattice, how are the local Wannier orbital states of fractional particles characterized when they undergo hopping under tight-binding (TB) gauge fields? Standard methods such as maximally localized Wannier orbitals [23–25], perturbation theory [26–32], renormalized Hamiltonian [33], rotating-wave approximation [34,35], and Hubbard-Stratonovich transformation [36,37] produce effective low-energy models for conventional quasiparticles hopping in a lattice potential. In contrast, entangled or fractional particles traverse a lattice under a lattice gauge potential. Symmetry arguments and dualities are often employed to postulate such lattice gauge theory coupled with particle excitations [9,38–41]. Wegner realized that the high-temperature disorder phase of the Ising excitations is dual to a $\mathbb{Z}_2$ lattice gauge theory [42]. Kitaev introduced an exactly solvable low-energy spin model exhibiting a spin-liquid ground state, which directly translates to a $\mathbb{Z}_2$ lattice gauge theory [43–46]. However, a systematic derivation of an effective $\mathbb{Z}_2$ gauge-field-mediated TB model for the low-energy states for fractional particles that are embedded in a larger Hilbert space is lacking in the literature.

Published by the American Physical Society under the terms of the Creative Commons Attribution 4.0 International license. Further distribution of this work must maintain attribution to the author(s) and the published article's title, journal citation, and DOI.

Conventional approaches to eliminating high-energy states typically involve projecting onto a low-energy subspace, but this method can introduce limitations such as Wannier obstructions to localization and constraints on correlations. In this work, we present a novel framework that circumvents these issues by applying the projection operator to the Hamiltonian rather than the states. We start with a Wannier orbital ansatz without direct projection, instead incorporating the projection operator and a variational geometric potential directly into the Hamiltonian. This allows us to extract the TB gauge field and quantum metric through a superexchange mechanism. Importantly, the method facilitates the imposition of a flux-preservation constraint, ensuring consistency between the global topology in the extended states and the uniform flux phase in the local orbital states of the fractional particles. Additionally, higher-order virtual hopping processes naturally give rise to quartic interactions between fractional orbitals, which we solve via a gauge-invariant mean-field theory.

We apply our framework to investigate Majorana orbitals in $\mathbb{Z}_2$ gauge fields in the Kitaev spin-1/2 model on the honeycomb lattice [43]. The model, known for its exact solution, exhibits uniform $\mathbb{Z}_2$ fluxes in the ground state and Majorana fermions as excitations. With an applied magnetic field [47–53], the Majorana excitations can proliferate, leading to flux crystallization [54–57] and their glassiness [19]. In the flux-crystalline phase, the model remains nearly exactly solvable, resulting in dispersive Majorana bands that have been extensively studied in the literature [54–64]. These Majorana bands exhibit transitions between gapless and gapped behavior depending on the flux configurations and also feature flat bands with integer Chern numbers. Our work advances beyond these studies by (1) deriving an effective low-energy $\mathbb{Z}_2$ gauge theory via superexchange mechanism, and constructing Wannier Majorana orbitals that evade obstructions, (2) investigating the quantum geometry, including the quantum metric and topology across the flat-Majorana dispersion phase, (3) developing a gauge-invariant mean-field theory to describe geometry-induced interaction effects between fractional orbitals, and (4) proposing an analytical model for fractional Chern states.

The derived lattice model for Majorana orbitals with $\mathbb{Z}_2$ gauge fields reproduces the low-energy band structure. To ensure topological consistency, we fix the gauge with a uniform flux per unit cell, guaranteeing an integer Chern number in the extended Majorana states. Notably, we find an interesting topological phase transition with a flat band degeneracy at the critical point, distinct from conventional topological phase transitions, involving band gap closing at a Dirac point or nodal line degeneracy. The presence of flat bands allows for the emergence of fractional Chern bands for interacting Majorana fermions. To describe this phenomenon, we introduce a mean-field theory for the gauge-invariant Majorana density-wave state in the flat bands, providing an analytically tractable description of a fractional Chern insulator state. This mean-field analysis offers valuable analytical insights into the general "trace" or "vortexibility" condition for fractional Chern states in flat bands [65].

II. KITAEV MODEL WITH STAGGERED FLUXES

The Kitaev model is a particular lattice model of the spin-1/2 fields $\mathbf{S}_i$ sitting at the ith site on a honeycomb lattice and interacting with the nearest neighboring sites with bond-dependent exchange coupling J. A magnetic field of strength h is applied along the [111] direction, giving the corresponding model as [43]

$$H = -J \sum_{\alpha=x,y,z,\langle ij\rangle_\alpha} S_i^\alpha S_j^\alpha - h \sum_{i,\alpha=x,y,z} S_i^\alpha. \tag{1}$$

In the Majorana fermion representation $S_i^\alpha = i b_i^\alpha c_i$, the model reduces to a model of nearest-neighbor Majorana (c_i) hoppings mediated by a bond-dependent $\mathbb{Z}_2$ gauge field $u_{ij} = i b_i^\alpha b_j^\alpha = \pm 1$. For a small magnetic field h, the lowest-order perturbation term produces a next nearest-neighbor hopping with the coupling constant $K \sim h^3/J^2$ (from the term $\sum_{\langle\langle ik\rangle\rangle} S_i^y S_j^z S_k^x$) [43,59,66–71]. The model is expressed as

$$H = iJ \sum_{\langle ij\rangle} u_{ij} c_i c_j + iK \sum_{\langle\langle ik\rangle\rangle} u_{ij} u_{jk} c_i c_k. \tag{2}$$

The candidacy of the gauge field u_{ij} demands it to be an antisymmetric tensor: $u_{ij} = -u_{ji}$, living on the bond between the i and j sites. And the gauge field for the next-nearest neighbor u_{ik} is a path-ordered product of two subsequent nearest-neighbor gauge fields $u_{ik} = u_{ij} u_{jk}$, where j is the intermediate site between i and k. This is reflected in the second term in Eq. (2). A gauge choice of u_{ij} is shown in Fig. 1(b). A $\mathbb{Z}_2$ operator, defined on six consecutive links forming a loop on a plaquette p, is defined as $W_p = u_{ij} u_{jk} u_{kl} u_{lm} u_{mn} u_{ni}$. W_p gives the $\mathbb{Z}_2$ flux monopole charge with $W_p = \pm 1$ for zero (π) flux. Another flux operator of importance is defined at the rth site (called a vertex) as $X_r = u_{rs} u_{rt} u_{rq}$, where t, s, q are the nearest-neighbor site indices of the site r, which acts as a $\mathbb{Z}_2$ electric charge, and introduces quartic interaction between Majoranas (see Sec. IV D).

The Hamiltonian's gauge redundancy manifests in gauge-dependent Majorana dispersions. However, the essential properties of these dispersions, such as the presence of gapless point (point degeneracy), flat band (extensive degeneracy), or topological features (band inversions), are gauge invariant. The specific location of these gapless or band inversion points depends on the chosen gauge. In uniform flux configuration with all

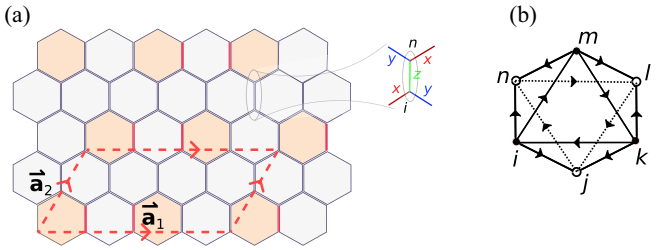


FIG. 1. $\mathbb{Z}_2$ flux crystal structure and the supercell formation in the Kitaev model. (a) We show a 2×2 supercell of honeycomb lattice containing a π-flux ($W_p=-1$) pair (orange plaquette) separated by two vertical bonds having $u_{ij}=-1$, while the rest of the plaquettes (white) have zero flux and bonds have $u_{ij}=+1$. $\mathbf{a}_1=(4a\sqrt{3},0)$ and $\mathbf{a}_2=a(\sqrt{3},3)$, where a is the nearest-neighbor distance in the honeycomb lattice. Inset: three different exchange interactions with equal strength J, along the three nearest neighbors at each site are highlighted in different colors. (b) The chosen gauge convention for the u operators in the Kitaev model is shown as $u_{ij}=+1$ if an arrow points from the site i to j, or -1 otherwise. The same is shown for the next-nearest neighbors by dashed lines where two u operators for the intervening nearest-neighbor bonds are multiplied. For example, the bond from the site i to k term has $u_{ij}u_{jk}=-1$. This convention is for the uniform flux sector, where each plaquette has zero flux.

$W_p=+1$ and a gauge fixing of all $u=+1$, we obtain a graphene dispersion with gapless Dirac node for $K=0$. $K\neq 0$ breaks the time-reversal symmetry, opening a band gap at the Dirac cone to topological Chern bands for Majorana fermions. This topological phase has Majorana zero modes (MZMs) at the boundary. Bound states of MZM with π-flux excitations can be created in bulk by thermal energy or vacancies. MZMs are topologically protected Ising anyons, which can be detected by thermal probes [72] and by scanning tunneling microscopic techniques [73].

The focus of this work is to study different supercell formations of staggered W_p fluxes and their impact on low-energy Majorana dispersions [56,60–64]. Analogous to the U(1) magnetic monopole, a $\mathbb{Z}_2$ monopole W_p is topologically protected. A $\mathbb{Z}_2$ flux pair is defined by two π fluxes separated by d number of plaquettes with $u=-1$ in the intermediate links, as shown in Fig. 1(a). There is gauge redundancy in defining the supercell, and we fix the gauge for all considered supercells in the same way, as shown in Fig. 1(b). This produces a $d\times d$ supercell of honeycomb lattice containing $2N=4d^2$ number of Majorana sublattices. A $\mathbb{Z}_2$ flux pair for $d>1$ naturally breaks the C_6 symmetry of the honeycomb lattice; however, the alignments of the $\mathbb{Z}_2$ flux pair along, say, either $\mathbf{a}_1$ or $\mathbf{a}_2$ primitive lattice vectors, are gauge equivalent.

We chose a Majorana spinor $C_I=(c_1c_2\ldots c_{2N})^T$ at the Ith supercell site. Then the matrix-valued Hamiltonian in this spinor can be written from Eq. (2) as

$$H=i\sum_I C_I^T\mathcal{T}_{II}C_I+i\sum_{\langle IJ\rangle}C_I^T\mathcal{T}_{IJ}C_J. \tag{3}$$

Here, the $\mathcal{T}_{IJ}$ is a rank-2 tensor, with each element being a $2N\times 2N$ antisymmetric matrix. Their explicit forms are given in Appendix A. The basis vectors of the supercell are $\mathbf{a}_1=2da(\sqrt{3},0)$, $\mathbf{a}_2=[(da)/2](\sqrt{3},3)$, where a is the nearest-neighbor distance of the honeycomb primitive unit cell. The corresponding reciprocal vectors are $\mathbf{G}_1=[(2\pi)/a]\{[\sqrt{3}/(6d)],[-1/(6d)]\}$, $\mathbf{G}_2=[(2\pi)/a]\{0,[2/(3d)]\}$. The $\mathbf{a}_2$ vector of these supercells is half compared to the C_6 symmetric honeycomb lattice; see Fig. 1(a). Hence, the first Brillouin zone has two graphene BZs along the $\mathbf{G}_2$ vector.

The (virtual) Majorana spinor state in the momentum space is $C(\mathbf{k})=(1/\sqrt{L})\sum_I e^{-i\mathbf{k}.\mathbf{R}_I}C_I$, where $\mathbf{R}_{I\in\mathbb{Z}}=\sum_i I_i\mathbf{a}_i$ are the lattice sites of the supercell, and correspondingly, $\mathbf{k}$ is defined in the reciprocal space of $\mathbf{G}_{1,2}$. The corresponding Hamiltonian in the momentum space is obtained from Eq. (3): $H=(1/\sqrt{N})\sum_{\mathbf{k}\in \mathrm{BZ}_+}C^\dagger(\mathbf{k})\mathcal{H}(\mathbf{k})C(\mathbf{k})$, where the matrix elements of $\mathcal{H}$ are given in Appendix A. The physical Majorana fermions $c_i=c_i^\dagger$ turn into particle-hole symmetric virtual Majorana fermions in the $\mathbf{k}$ space $c^\dagger(\mathbf{k})=c(-\mathbf{k})$, leading to $\mathbf{k}\geq 0$ being restricted to the positive quadrant in the first Brillouin zone (BZ_+). The final task is to diagonalize the $2N\times 2N$ particle-hole symmetric matrix $\mathcal{H}(\mathbf{k})$. We denote the eigenvector states as $|n,\pm,\mathbf{k}\rangle$ corresponding to the eigenvalues of $\pm E_n(\mathbf{k})$, where $n=1,2,\ldots,N$. In this eigenbasis, the matter fields are the complex fermions (particles and holes), and related to the virtual Majoranas by a unitary transformation as discussed in Appendix B. The corresponding results are presented in Sec. IV for several representative $d\times d$ supercell configurations.

III. TIGHT-BINDING GAUGE-FIELD MODEL FOR MAJORANA ORBITALS

Our task now is to obtain an effective TB model for a few low-energy eigenstates $|n,\pm,\mathbf{k}\rangle$. Since $|n,\pm,\mathbf{k}\rangle$ states are for complex fermions, we may treat the corresponding Wannier orbitals to be of the usual complex fermionic nature. However, owing to the underlying physics of Majorana Wannier orbitals hopping under lattice $\mathbb{Z}_2$ gauge field in real space, the TB model construction becomes nontrivial. In essence, we need to construct "Wannier" fields for both Majorana matter fields and the $\mathbb{Z}_2$ gauge fields while keeping all the symmetries and flux-preservation constraints intact.

To avoid overloading with many new symbols, for the TB model, we adopt the same set of symbols, such as $\mathcal{H}$, $\mathcal{T}$, c, C and others used in the above Sec. II with the same meanings. Should confusion arise, we explicitly mention the corresponding definition.

We are interested in modeling the $P<N$ number of low-energy Majorana pair states $|p,\pm,\mathbf{k}\rangle\equiv|\mathbf{p},\mathbf{k}\rangle$, where we

combine the indices $\mathbf{p} \equiv (p, \pm)$ for $p = 1, \ldots, P$ with eigenvalues $\pm E_p(\mathbf{k})$. These states are obtained from the full Hilbert space $|\mathbf{n} \equiv (n, \pm), \mathbf{k}\rangle$ by the projector $\mathcal{P} = \mathcal{P}_+ + \mathcal{P}_- = \sum_{p<N} (|p, +\rangle\langle p, +| + |p, -\rangle\langle p, -|)$, where $\mathbf{k}$ dependence in each term is kept implicit for simplicity in notation. $\mathcal{Q} = I - \mathcal{P}$ is the projection outside the low-energy states of our interest. Since $|\mathbf{p}, \mathbf{k}\rangle$ states are incomplete, their Fourier transformation to the Wannier orbitals in real space would not be useful.

Our aim is to obtain complete, orthogonal states denoted by $|\tilde{\mathbf{p}}, \mathbf{k}\rangle$ with corresponding eigenenergies $\tilde{E}_p(\mathbf{k}) \approx E_p(\mathbf{k})$. One typically defines a complex quantum geometric tensor from the $\mathcal{Q}$ projector and affixes it with the $|\mathbf{p}, \mathbf{k}\rangle$ states to obtain corresponding complete, orthogonal states $|\tilde{\mathbf{p}}, \mathbf{k}\rangle$ (with a quantum metric) [23,74–79]. Here, we devise an alternative bottom-up approach to construct a (variational) effective Hamiltonian H_{eff} with eigenstates $|\tilde{\mathbf{p}}, \mathbf{k}\rangle$ and eigenenergies $\pm\tilde{E}_{\mathbf{p}}(\mathbf{k})$. We introduce a superexchange interaction that produces tunneling between $|\mathbf{p}, \mathbf{k}\rangle$ and $|\mathbf{p}', \mathbf{k}\rangle$ states with intermediate hopping to the $\mathcal{Q}$ states; see Fig. 2. We call such a superexchange potential a "gauge" potential, through which we can define the $\mathbb{Z}_2$ gauge fields and topology in a lattice.

In what follows, we seek an effective Majorana Hamiltonian of the form $H_{\text{eff}} = \mathcal{P}(H + H')\mathcal{P}$, $\forall$ $\mathbf{k}$, where H is the full supercell Hamiltonian and H' is an unknown superexchange or gauge potential to be evaluated self-consistently. H' gives off-diagonal terms in H_{eff} arising from the transitions between different Majorana states $|\boldsymbol{p} = (p, \pm), \mathbf{k}\rangle$ via intermediate hopping to the $\mathcal{Q}$ states. Since H_{eff} is a Hermitian matrix, its Hilbert space is complete. We denote the corresponding complete basis states by $|\boldsymbol{\alpha} = (\alpha, \pm), \mathbf{k}\rangle$ for $\alpha = 1, \ldots, P$. In the basis of $|\alpha, +, \mathbf{k}\rangle \oplus |\alpha, -, \mathbf{k}\rangle$, we denote the matrix elements of $H_{\text{eff}}(\mathbf{k})$ as

$$\mathcal{H}_{\text{eff}}(\mathbf{k}) = \begin{pmatrix} \Delta_R & \Delta_I + ih_S \\ \text{H.c.} & -\Delta_R \end{pmatrix}, \tag{4}$$

where $\mathbf{k}$ dependence on rhs is kept implicit. $h_S(\mathbf{k}) = h(\mathbf{k}) + h^T(-\mathbf{k})$, and $\Delta(\mathbf{k}) = \Delta_R(\mathbf{k}) + i\Delta_I(\mathbf{k})$. Here, we restrict $\mathcal{H}_{\text{eff}}$ to this particular form with the goal of obtaining Majorana orbitals, though a more general form could be considered for other types of excitations. The diagonal and off-diagonal $P \times P$ matrices of $\mathcal{H}_{\text{eff}}$ are relabeled in terms of h and Δ, so that the corresponding Hamiltonian in the complex fermion basis turns into a Bogolyubov–de Gennes Hamiltonian with h and Δ being their dispersion and pairing terms [43,80]. The block-off-diagonal term $(\Delta_I + ih_S)_{\alpha,\alpha'}$ couples different Majoranas $|\alpha, \pm, \mathbf{k}\rangle$ and $|\alpha', \mp, \mathbf{k}\rangle$, while the block-diagonal terms $\pm(\Delta_R)_{\alpha,\alpha'}$ give the dispersion for the same type of Majoranas $|\alpha, \pm, \mathbf{k}\rangle$ and $|\alpha', \pm, \mathbf{k}\rangle$. $\mathcal{H}_{\text{eff}}$ follows all the symmetries of the original Hamiltonian; in addition, the fermion odd parity in the pairing term Δ is also imposed. Explicit expressions of h and Δ in terms of H and H' are derived in Appendix B.

Our next task is to Fourier transform H_{eff} to real space by converting h and Δ into $\mathbb{Z}_2$ gauge-field-induced hoppings between Wannier Majorana orbitals in a lattice. We consider a lattice of $\mathcal{N}$ unit cells at positions $\mathbf{R}$. The Fourier basis states are the Bloch phases at the $\mathbf{R}$th cell as $z_{\mathbf{R}}(\mathbf{k}) = \langle \mathbf{R}|\mathbf{k}\rangle = e^{i\mathbf{k}\cdot\mathbf{R}}$. Then we define the Majorana orbital states in real space as

$$|\boldsymbol{\alpha}, \mathbf{R}\rangle = \frac{1}{\sqrt{\mathcal{N}}} \sum_{\mathbf{k}>0} \bar{z}_{\mathbf{R}}(\mathbf{k}) |\boldsymbol{\alpha}, \mathbf{k}\rangle. \tag{5}$$

The physical Majorana operators are defined in real space as $|\boldsymbol{\alpha}, \mathbf{R}\rangle = c_{\boldsymbol{\alpha},\mathbf{R}}|0\rangle$ where $c_{\boldsymbol{\alpha},\mathbf{R}} = c^\dagger_{\boldsymbol{\alpha},\mathbf{R}}$. The corresponding orthogonal Majorana wave functions at position $\mathbf{r} \in \mathbf{R}$ unit cell are called the Bloch states $\psi_{\boldsymbol{\alpha},\mathbf{k}}(\mathbf{r}) = e^{i\mathbf{k}\cdot\mathbf{r}} u_{\boldsymbol{\alpha},\mathbf{k}}(\mathbf{r}) = \langle \mathbf{r}|\boldsymbol{\alpha}, \mathbf{k}\rangle$, and Wannier states $w_{\boldsymbol{\alpha},\mathbf{R}}(\mathbf{r}) = \langle \mathbf{r}|\boldsymbol{\alpha}, \mathbf{R}\rangle$. In the TB orbital case, the real-space wave functions are fully localized to $w_{\boldsymbol{\alpha},\mathbf{R}}(\mathbf{r}) \sim \delta(\mathbf{r} - \mathbf{R})$. In the Wannier orbital model $w_{\boldsymbol{\alpha},\mathbf{R}}$ is (exponentially) maximally localized at $\langle \mathbf{r} \rangle_{\boldsymbol{\alpha}} = \int_{\mathbf{R}} d\mathbf{r} \mathbf{r} |w_{\boldsymbol{\alpha},\mathbf{R}}(\mathbf{r})|^2$, with its spread $\Delta \mathbf{r}_{\boldsymbol{\alpha}} = \langle \mathbf{r}^2 \rangle_{\boldsymbol{\alpha}} - \langle \mathbf{r} \rangle^2_{\boldsymbol{\alpha}}$ also contained within the unit cell (see Appendix C). The two particle-hole Majorana pairs may have different Wannier centers $\langle \mathbf{r} \rangle_{\alpha,+} \neq \langle \mathbf{r} \rangle_{\alpha,-}$, generally connected by a string $\mathbb{Z}_2$ vortex. However, their linear combination gives particle-hole complex fermion wave function which must be at the

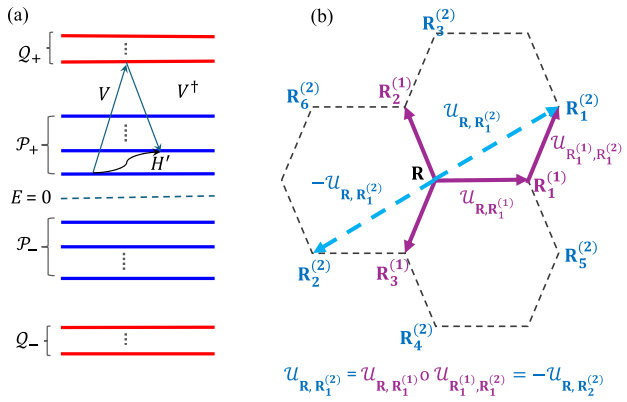


FIG. 2. (a) Schematic plots of the superexchange mechanism of gauge potential H' in the low-energy spectrum (blue lines) due to virtual hopping to the eliminated high-energy states (red lines). Note that the virtual hopping potential V is a fitting parameter in the TB model. (b) The gauge fields in the effective theory in a honeycomb lattice. The sets of first and second nearest-neighbor sites are denoted by $\{\mathbf{R}^{(1)}_{1-3}\}$ and $\{\mathbf{R}^{(2)}_{1-6}\}$. The gauge field for the second nearest neighbor across diagonally opposite directions must be opposite in sign to commence odd-parity hopping [superconducting term in Eq. (B3); i.e., $\mathcal{U}_{\mathbf{R},\mathbf{R}_2^{(1)}} = -\mathcal{U}_{\mathbf{R},\mathbf{R}_1^{(2)}}$].

same position such that the U(1) charge is conserved in each unit cell.

It is convenient to represent the $\mathbf{R}$ positions in terms of sets of first, second, third, and higher nearest neighbors rather than primitive lattice vectors. For the nth nearest neighbor with d_n number of sites (called coordination number), we define a d_n-dimensional vector as $\mathbf{Z}_n \coloneqq (z_1 \ldots z_{d_n})^T$, $\forall\ \mathbf{k}$. We split the $\mathcal{N}$-dimensional vector of the Bloch phases as $\mathbf{Z}(\mathbf{k}) = \mathbf{Z}_1(\mathbf{k}) \oplus \mathbf{Z}_2(\mathbf{k}) \oplus \cdots$ [81,82].

We now expand the dispersion relations in the Bloch basis $\mathbf{Z}(\mathbf{k})$ to obtain the TB hopping tensor as $\mathcal{T} = \mathbf{Z}(\mathbf{k})\mathcal{H}_{\text{eff}}(\mathbf{k})\mathbf{Z}^\dagger(\mathbf{k})$. $\mathcal{T}$ is a rank-2 tensor with component $\mathcal{T}_{\mathbf{R},\mathbf{R}'}$ corresponding to Majorana hoppings between $\mathbf{R}, \mathbf{R}' \in \mathcal{N}$ sites. [Here, the symbol $\mathcal{T}$ is redefined for the Wannier states and not to be confused with those in the supercell in Eq. (3).] Each tensor component $\mathcal{T}_{\mathbf{R},\mathbf{R}'}$ is a $2P \times 2P$ matrix in the $2P$-dimensional Majorana basis present at the $\mathbf{R}, \mathbf{R}'$ sites. We split the Hamiltonian into hoppings between different neighboring sites n, n' as

$$\mathcal{H}_{\text{eff}}(\mathbf{k}) = \sum_{n,n'} \mathbf{Z}_n^\dagger(\mathbf{k}) \mathcal{T}_{nn'} \mathbf{Z}_{n'}(\mathbf{k}) + \text{H.c.} \tag{6}$$

$\mathcal{T}_{nn'}$ gives a set of Majorana hopping tensors between the n and n' neighbors: $\mathcal{T}_{n,n'} = \{\mathcal{T}_{\mathbf{R},\mathbf{R}'} | \mathbf{R} \in d_n, \mathbf{R}' = \in d_{n'}\}$. Because of the translational invariance, only the difference between n and n' is relevant.

The intrasite hopping gives the on-site energy $\mathcal{T}_{nn} = i\mathcal{K}_0$ between $2P$ Majoranas with the particle-hole symmetric constraint $\text{Tr}(\mathcal{T}_{nn}) = 0$.

Now, we consider the first nearest-neighbor term $\mathcal{T}_{\mathbf{R},\mathbf{R}'} \in \mathcal{T}_{n,n+1}$, where $\mathbf{R}' - \mathbf{R} \in d_1$ and $\mathbf{R} \neq \mathbf{R}'$. Using Taylor's expansion (assuming analyticity), we obtain the hopping tensor as

$$\mathcal{T}_{\mathbf{R},\mathbf{R}'} = i\mathcal{K}_1^{-1} \frac{\partial^2 \mathcal{H}_{\text{eff}}}{\partial \bar{z}_{\mathbf{R}} \partial z_{\mathbf{R}'}}\bigg|_{z_{\mathbf{R}} = z_{\mathbf{R}'} = 0}. \tag{7}$$

$\mathcal{K}_1$ is, in general, orbital dependent ($2P \times 2P$ nonsingular matrices) as well as bond (i.e., $\mathbf{R}, \mathbf{R}'$) dependent. [This expansion holds when $\mathcal{H}_{\text{eff}}$ are polynomials in terms of $z_{\mathbf{R}}(\mathbf{k})$, which holds for most band structures, except for noncompact flat bands [83,84].] $\mathcal{K}_1$ absorbs the energy dimension such that $\mathcal{T}_{\mathbf{R},\mathbf{R}'}$ becomes dimensionless, which is now to be defined in terms of gauge fields. The crux of the gauge theory is that $\mathcal{T}_{\mathbf{R},\mathbf{R}'} \neq \mathcal{T}_{\mathbf{R}',\mathbf{R}}$ in general. We separate the symmetric and antisymmetric parts as

$$\mathcal{G}_{\mathbf{R},\mathbf{R}'} = \frac{1}{2}(\mathcal{T}_{\mathbf{R},\mathbf{R}'} + \mathcal{T}_{\mathbf{R}',\mathbf{R}}), \tag{8}$$

$$\mathcal{U}_{\mathbf{R},\mathbf{R}'} = -\frac{i}{2}(\mathcal{T}_{\mathbf{R},\mathbf{R}'} - \mathcal{T}_{\mathbf{R}',\mathbf{R}}). \tag{9}$$

Roughly speaking, $\mathcal{G}$ and $\mathcal{U}$ produce the amplitude and phase variation of the hopping term in H_{eff} between $\mathbf{R}$ and $\mathbf{R}'$. In the momentum space, these are precisely the Fubini-Study metric ($\mathcal{G}_{\mu\nu}$) and the curvature ($\mathcal{U}_{\mu\nu}$) terms are, which constitute the symmetric and antisymmetric components of the quantum geometric tensor [75,76,85,86]. Their expressions in terms of the projector $\mathcal{P}(\mathbf{k})$ are as follows:

$$\mathcal{G}_{\mu\nu}(\mathbf{k}) = \frac{1}{2}\mathcal{P}(\mathbf{k})\{\partial_\mu \mathcal{P}(\mathbf{k}), \partial_\nu \mathcal{P}(\mathbf{k})\}, \tag{10}$$

$$\mathcal{U}_{\mu\nu}(\mathbf{k}) = -\frac{i}{2}\mathcal{P}(\mathbf{k})[\partial_\mu \mathcal{P}(\mathbf{k}), \partial_\nu \mathcal{P}(\mathbf{k})], \tag{11}$$

where $\partial_\mu = [\partial/(\partial k_\mu)]$ with $\mu = 1, 2$ for $\mathbf{k}_\mu$ spanned along the reciprocal lattice vector $\mathbf{G}_\mu$. $\{\}$ and $[]$ are the anticommutator and commutator. It is now obvious that $\mathcal{U}$ acts as parallel transport or Wilson line, which is $\mathbb{Z}_2$ valued in our case. In their present forms, $\mathcal{G}$ and $\mathcal{U}$ are not gauge invariant in both real and momentum space formalism. Then, matter fields are attached at the two ends to commence gauge invariance. Otherwise, we take a trace over the matrix components and their product in a loop or plaquette in real or momentum space, giving topological invariants such as flux (W) or monopole in real space, Chern number (C) in momentum space, and similar quantum metric invariants as defined in Sec. IV C.

The diagonal term of $\mathcal{G}$ tensor is zero as the $\mathbf{R} = \mathbf{R}'$ terms are separated into the on-site energy matrix $\mathcal{K}_0$. The off-diagonal components $\mathcal{G}_{\mathbf{R},\mathbf{R}'}$ give the symmetric hopping matrix element between the orbitals localized at $\mathbf{R}$ and $\mathbf{R}'$ sites. Such symmetric hoppings are mediated by periodic lattice potential (e.g., potential due to nucleus in solid-state systems) and depend on the symmetries of the two orbitals (e.g., it is present if the two orbitals have the same parity or absent if the parity of the two orbitals is opposite such as for the s and p orbitals [87]). In our particular example below, we seek a fully gauge-field-mediated hopping between the two sites and set $\mathcal{G} = 0$ in the effective theory.

So far, we have kept the formalism general for any quasiparticles under U(1) or SU(N) gauge fields. From now on, we impose the $\mathbb{Z}_2$ symmetry on the gauge fields for Majorana quasiparticles. We identify $\mathcal{U}_{\mathbf{R},\mathbf{R}'}$ as an antisymmetric tensor that mediates tunneling between the Majoranas at the $\mathbf{R}$ and $\mathbf{R}'$ sites. For the gauge invariance of the theory for Majorana, the gauge fields must be $\mathbb{Z}_2$, which puts the constraints that $\mathcal{U}_{\mathbf{R},\mathbf{R}'}^2 = \mathbb{I}$. So we interpret $\mathcal{U}_{\mathbf{R},\mathbf{R}'}$ as the non-Abelian ($2P$-dimensional matrix-valued) $\mathbb{Z}_2$ Wilson line operator, which can be written as (path-ordered) exponentials of a (non-Abelian) gauge field $\mathcal{A}$.

Next, we consider the second nearest-neighbor term $\mathcal{T}_{\mathbf{R},\mathbf{R}''} \in \mathcal{T}_{n,n+2}$, where $\mathbf{R}'' - \mathbf{R} \in d_2$ and $\mathbf{R} \neq \mathbf{R}''$. Proceeding similarly, we define the $\mathbb{Z}_2$ gauge field as the second nearest neighbor as $\mathcal{U}_{\mathbf{R},\mathbf{R}''}$. All gauge fields $\mathcal{U}$ are localized at the link or bond between the two sites.

So we can smoothly deform the path to pass through a site $\mathbf{R}'$ corresponding to the first nearest neighbor to both $\mathbf{R}$ and $\mathbf{R}''$ sites, as shown in Fig. 2. In other words, we can write $\mathcal{U}_{\mathbf{R},\mathbf{R}''} = \mathcal{U}_{\mathbf{R},\mathbf{R}'} \circ \mathcal{U}_{\mathbf{R}',\mathbf{R}''}$, where the composition operation $\circ$ reflects a matrix product for the tensor components. Therefore, for the nth-nearest-neighbor gauge field, we have

$$\mathcal{U}_{\mathbf{R},\mathbf{R}^{(n)}} = \prod_{\mathbf{R}^{(m)} \in d_{n-1}} \mathcal{U}_{\mathbf{R},\mathbf{R}^{(m)}} \circ \mathcal{U}_{\mathbf{R}^{(m)},\mathbf{R}^{(n)}}, \tag{12}$$

where $\mathbf{R}^{(m)}$ runs over the $n-1$ intermediate sites that minimize the distance between the $\mathbf{R}$ and $\mathbf{R}^{(n)}$ sites. Substituting these considerations in Eq. (6) we get

$$\begin{aligned}\mathcal{H}_{\text{eff}}(\mathbf{k}) = i\mathcal{K}_0 + i\mathcal{K}_1 \sum_{\{\mathbf{R},\mathbf{R}^{(1)}\} \in d_1} \mathcal{U}_{\mathbf{R},\mathbf{R}^{(1)}} \bar{z}_{\mathbf{R}}(\mathbf{k}) z_{\mathbf{R}^{(1)}}(\mathbf{k}) \\ + i\mathcal{K}_2 \sum_{\{\mathbf{R},\mathbf{R}^{(2)}\} \in d_2} \mathcal{U}_{\mathbf{R},\mathbf{R}^{(2)}} \bar{z}_{\mathbf{R}}(\mathbf{k}) z_{\mathbf{R}^{(2)}}(\mathbf{k}) + \cdots.\end{aligned} \tag{13}$$

The above Hamiltonian can be expressed in terms of physical Majorana orbitals $c_{\boldsymbol{\alpha},\mathbf{R}}$ in real space up to any number of nearest-neighbor ($\mathcal{N}$) hoppings as

$$\begin{aligned}H_{\text{eff}} = i \sum_{n=0}^{\mathcal{N}} \mathcal{K}_n \sum_{\{\mathbf{R},\mathbf{R}^{(n)}\} \in \mathbf{d}_n} \sum_{\boldsymbol{\alpha},\boldsymbol{\alpha}'} \\ \times (\mathcal{U}_{\mathbf{R},\mathbf{R}^{(n)}})_{\boldsymbol{\alpha},\boldsymbol{\alpha}'} c_{\boldsymbol{\alpha},\mathbf{R}} c_{\boldsymbol{\alpha}',\mathbf{R}^{(n)}}.\end{aligned} \tag{14}$$

Summation over n corresponds to different nearest neighbors. The gauge fields $\mathcal{U}_{\mathbf{R},\mathbf{R}^{(n)}}$ sit on the link between the $\mathbf{R}, \mathbf{R}^{(n)}$ sites, and hence, there is no gauge field for the $n = 0$ term, while $n = 1$ term has one gauge field, $n = 2$ has two gauge fields, and so on. Here, we have assumed the coupling constants $\mathcal{K}_n$ to be independent of the orbital and bond independent and only depending on the nth-nearest-neighbor distance. This is a reasonable assumption as at the nth-nearest-neighbor site, only one type of orbital is placed.

We note that the derivation of H_{eff} in Eq. (14) is quite general and can be extended for other fractional orbitals by relaxing the $\mathbb{Z}_2$ constraint on the gauge field and the particle-hole symmetry on the matter fields. Moreover, the evaluation of the parameters $\mathcal{T}_{\mathbf{R},\mathbf{R}'}$ in Eq. (7) and gauge fields in Eq. (8) does not necessitate the knowledge of the full spectrum of the original theory in Eq. (3). They can be treated as either fitting parameters if the excitation spectrum is known or variational parameters within a many-body wave function ansatz, though the latter approach is not explored in this work.

A. Gauge fixing and topological invariants

An important property of the gauge theory is the gauge constraint, which restricts gauge redundancy to the physical states. Although the gauge operators $\mathcal{U}_{\mathbf{R},\mathbf{R}^{(n)}}$ are gauge dependent, the flux is a gauge-invariant physical operator. Therefore, the total flux in the supercell must be preserved in both the effective model and the supercell model.

The total flux in a supercell is defined as $W_S = \prod_{p \in S} W_p$, where S is the supercell index containing S number of original unit cells. The W_S, written in terms of the effective $\mathbb{Z}_2$ gauge field, is

$$W_S = \text{Tr}\left(\prod_{\mathbf{R},\mathbf{R}^{(n)} \in S} \mathcal{U}_{\mathbf{R},\mathbf{R}^{(n)}} \right). \tag{15}$$

In the effective theory, we can define a similar invariant for the symmetric tensor $\mathcal{G}$ as $G_S = \text{Tr}(\prod_{\mathbf{R},\mathbf{R}^{(n)} \in S} \mathcal{G}_{\mathbf{R},\mathbf{R}^{(n)}})$.

Their counterparts in the momentum space are called the quantum metric invariant and the Chern number as defined to be [75,76,85,86]

$$G = \frac{1}{(2\pi)^2} \int_{\text{BZ}} \sqrt{\det(\eta)} \eta_{\mu\nu} dk_\mu dk_\nu \text{Tr}\mathcal{G}_{\mu\nu}(\mathbf{k}), \tag{16}$$

$$C = \frac{1}{2\pi} \int_{\text{BZ}} dk_1 dk_2 \text{Tr}\mathcal{U}_{12}(\mathbf{k}), \tag{17}$$

where $\eta_{\mu\nu} = \hat{\mathbf{G}}_\mu \cdot \hat{\mathbf{G}}_\nu$ is a symmetric tensor that measures the curvature of the torus geometry and depends on the lattice under consideration. W_S and G_S can describe both local and global topological properties in real space, depending on the size of the two-loop S. In contrast, C and G in the momentum space capture only the global topology on the torus. Do they correspond to the same topological invariant? Indeed, this is the case. Because the flux crystal in the original lattice is taken into account in the formation of the supercell, the total flux is uniform among all the supercells. This is reflected in the effective theory, as well, in that each band corresponds to uniform flux values $W_S = \pm 1, \ \forall \ S$, corresponding to Chern numbers $C = \pm 1$ for the two respective bands.

Both $\mathcal{G}_{\mu\nu}(\mathbf{k})$ and $\mathcal{U}_{\mu\nu}(\mathbf{k})$ can also be calculated directly from the effective Hamiltonian $\mathcal{H}_{\text{eff}}(\mathbf{k})$. The corresponding formulas appear similar by replacing $\mathcal{P}(\mathbf{k})$ with $\mathcal{H}_{\text{eff}}(\mathbf{k})$. For the Chern number, the formula coincides with the Kubo formula for Hall conductivity, while the same formula for G has no analog in any previous analysis. We compute them in Sec. IV C.

We consider $\mathcal{K}_n$ to be the TB hopping parameters related to the gauge potential H' in a self-consistent way to fit the low-energy band structure under an additional constraint of flux preservation. The values of the $\mathcal{K}_n$ parameters are the same as those obtained on the Wannier orbital basis, as shown below.

B. Examples of two Majorana bands in a honeycomb lattice

As an example, appropriate for the Kitaev model of present interest, we consider a honeycomb lattice with one

($P = 1$) pair of Majorana bands; see Fig. 2(b). Here we have $d_1 = 3$ first nearest neighbors $\mathbf{R}^{(1)} - \mathbf{R} = \delta\mathbf{R}^{(1)} = \{\frac{1}{2}(1, \pm\sqrt{3}), (-1, 0)\}$ and $d_2 = 6$ second nearest neighbors $\mathbf{R}^{(2)} - \mathbf{R} = \delta\mathbf{R}^{(2)} = \{\pm\frac{1}{2}(3, \sqrt{3}), \pm\frac{1}{2}(3, -\sqrt{3}), \pm(0, -\sqrt{3})\}$, and so on.

Since only one type of Majorana orbital is positioned at each site, we can split the position and orbital indices from the gauge field as $\mathcal{U}_{\mathbf{R},\mathbf{R}'} = u_{\mathbf{R},\mathbf{R}'}\boldsymbol{\sigma}$. Here $u_{\mathbf{R},\mathbf{R}'} = \pm 1$, and $u_{\mathbf{R},\mathbf{R}'} = -u_{\mathbf{R}',\mathbf{R}}$ are the $\mathbb{Z}_2$ gauge fields for two orbitals positions at $\mathbf{R}$, and $\mathbf{R}'$ sites, and $\boldsymbol{\sigma}$ are the Pauli matrices in two ($a = \pm$) Majorana basis. In this bipartite lattice, the same (different) Majorana orbitals are positioned at the first (second) nearest-neighbor sites. Hence, the first nearest-neighbor gauge field is off diagonal: $\mathcal{U}_{\mathbf{R},\mathbf{R}^{(1)}} = u_{\mathbf{R},\mathbf{R}^{(1)}}\sigma^x$. The second nearest neighbor is diagonal $\mathcal{U}_{\mathbf{R},\mathbf{R}^{(2)}} = u_{\mathbf{R},\mathbf{R}^{(1)}} u_{\mathbf{R}^{(1)},\mathbf{R}^{(2)}}\sigma^z$, where $\mathbf{R}^{(1)}$ is the first nearest neighbor that connects $\mathbf{R}$ and $\mathbf{R}^{(2)}$ sites in the shortest distance. In all the diagonal terms, $a = \pm$ orbitals must have opposite gauge fields for the Hamiltonian to be particle-hole symmetric, and hence, we have σ^z here.

Taking into account the above properties, we have the TB Majorana orbital Hamiltonian (up to the second nearest neighbors):

$$\begin{aligned} H_{\text{eff}} = {} & K_0 \sum_{\mathbf{R}} \sum_{a=\pm} c_{a,\mathbf{R}} \sigma^z_{aa'} c_{a',\mathbf{R}} \\ & + iK_1 \sum_{\mathbf{R},\mathbf{R}_i^{(1)} \in d_1} u_{\mathbf{R},\mathbf{R}_i^{(1)}} \sum_{a=\pm} c_{a,\mathbf{R}} \sigma^x_{aa'} c_{a',\mathbf{R}_i^{(1)}} \\ & + iK_2 \sum_{\mathbf{R},\mathbf{R}_j^{(2)} \in d_2} u_{\mathbf{R},\mathbf{R}_l^{(1)}} u_{\mathbf{R}_l^{(1)},\mathbf{R}_j^{(2)}} \sum_{a=\pm} c_{a,\mathbf{R}} \sigma^z_{aa'} c_{a',\mathbf{R}_j^{(2)}}. \end{aligned} \tag{18}$$

$u_{\mathbf{R},\mathbf{R}^{(1)}} = \pm 1$ can take any value in a link, provided the total flux in a unit cell is conserved to the value in the full Hamiltonian. $\mathcal{K}_i = K_i\mathbb{I}$ are set to be orbital-independent coupling constants for simplicity in notation in this example; however, in the fitting procedure in Sec. IV B they are considered orbital dependent. Going to the momentum space, we obtain the diagonal and off-diagonal terms as

$$\begin{aligned} \Delta_I(\mathbf{k}) + ih_S(\mathbf{k}) &= iK_1 \sum_{\mathbf{R},\mathbf{R}_i^{(1)} \in d_1} u_{\mathbf{R},\mathbf{R}_i^{(1)}} e^{i\mathbf{k}\cdot\delta\mathbf{R}_i^{(1)}}, \\ \Delta_R(\mathbf{k}) &= K_0 + iK_2 \sum_{\mathbf{R},\mathbf{R}_j^{(2)} \in d_2} u_{\mathbf{R},\mathbf{R}_l^{(1)}} u_{\mathbf{R}_l^{(1)},\mathbf{R}_j^{(2)}} e^{i\mathbf{k}\cdot\delta\mathbf{R}_j^{(2)}}. \end{aligned} \tag{19}$$

It is interesting to note here that the imaginary and real parts of the superconducting (complex-fermion) pairing gaps arise from the first and second nearest-neighbor Majorana hoppings, respectively.

Note that h_S, $\Delta_{R,I}$ are real. We set K_i to be real and $K_0 = 0$. This makes $\Delta_I = -2K_1 \sum_{i=1}^{3} \sin(\mathbf{k}\cdot\delta\mathbf{R}_i^{(1)})$, $h_S = -2K_1 \sum_{i=1}^{3} \cos(\mathbf{k}\cdot\delta\mathbf{R}_i^{(1)})$. Δ_R arises from the second next-nearest neighbor, which gives $-2K_2 \sum_{j=1,3,5} \sin(\mathbf{k}\cdot\delta\mathbf{R}_j^{(2)})$. This reduces the gauge choices for nearest neighbors to be $u_{\mathbf{R},\mathbf{R}_1^{(2)}} = -u_{\mathbf{R},\mathbf{R}_2^{(2)}}$, $u_{\mathbf{R},\mathbf{R}_3^{(2)}} = -u_{\mathbf{R},\mathbf{R}_4^{(2)}}$, and $u_{\mathbf{R},\mathbf{R}_5^{(2)}} = -u_{\mathbf{R},\mathbf{R}_6^{(2)}}$. This affects the gauge choices for the nearest neighbors and also the flux-modulation-induced supercell constructions, shown in Fig. 1. Both $\Delta_{R,I}$ are odd under spatial parity and are consistent with odd-fermion parity for the fermionic odd parity for complex fermion pairing for the same spin states. This gives the well-known $p + ip$ pairing state for the corresponding complex fermion state.

IV. RESULTS

A. Majorana band structure of the full supercell Hamiltonian

We consider here several representative superlattices of dimension $d \times d$ containing a single $\mathbb{Z}_2$ flux pair of length d, i.e., the number of $u = -1$ gauge fields flipped between the two $\mathbb{Z}_2$ fluxes, while $u = +1$ in the rest of the bonds in the supercell. This makes the supercell Hamiltonian dimension to be $2N = 4d^2$. A typical superlattice for $d = 2$ is shown in Fig. 1(a). It turns out the band structure properties are characteristically similar for all $3d \times 3d$ supercells, which differ from the characteristically similar band structure for other supercells. Therefore, we present the numerical results for two representative values of $d = 3$, 4 in Fig. 3 by diagonalizing the supercell Hamiltonian given in Eq. (3). We remind the reader that the band dispersion depends on the gauge choice; however, different gauge choices give equivalent dispersion along different momentum directions. Moreover, the salient properties such as gapless (degeneracy), gap, flat bands, Chern number, and quantum metric indices are gauge invariant. We show the gauge choice and the orientation of the $\mathbb{Z}_2$ flux pair for one example case of $d = 4$ in Fig. 4.

Interestingly, we find that only for the $d = 3$ (and its integer multiples) flux configuration, the Majorana dispersions are gapped even for $K = 0$, and render nearly flat band; see Fig. 3(a). The reason for the gapped behavior is the broken sublattice symmetry that protects the degeneracy at energy $E = 0$, although the particle-hole symmetry remains intact.

For other flux configurations, the Majorana bands show a gapless feature at energy $E = 0$ at the high-symmetric momenta for $K = 0$, a representative result of which is shown in Fig. 3(b). The low-energy particle-hole symmetric bands have linear dispersions around the gapless point, as in graphene, and also show linearly dispersing gap-closing points with high-energy bands. All these gapless points acquire mass term for $K \neq 0$ value; Fig. 3(c).

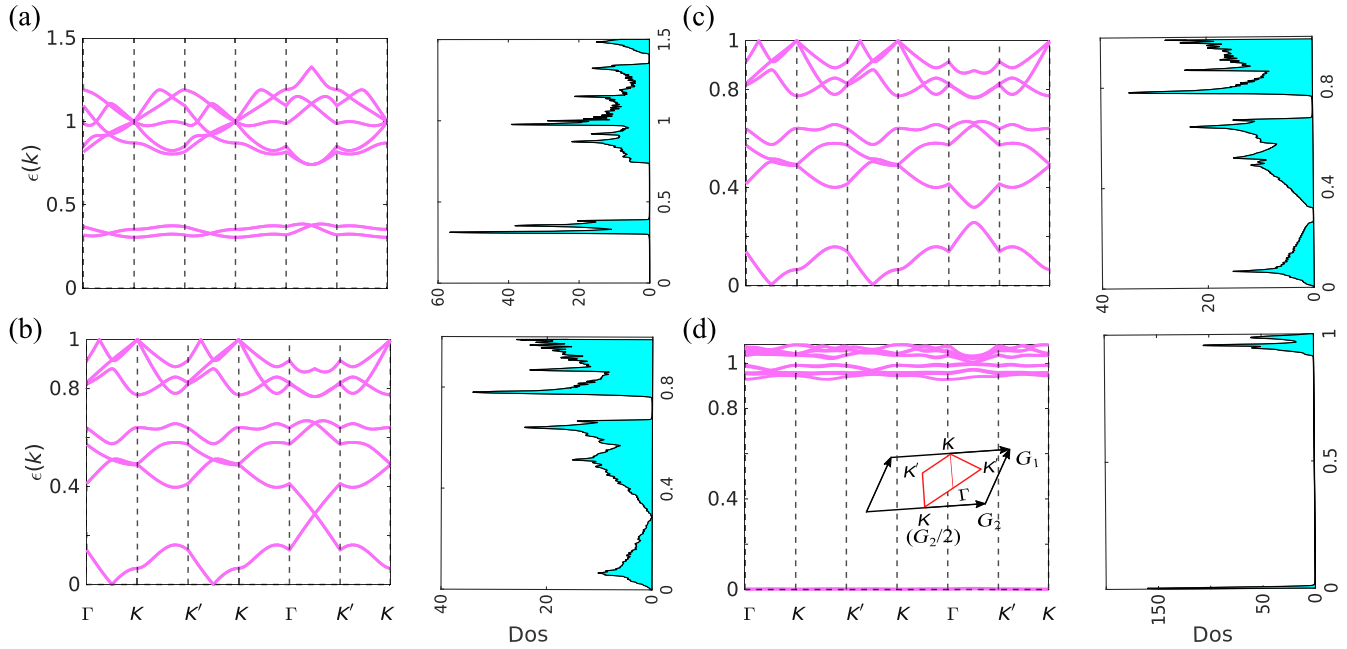


FIG. 3. The dispersions of the Majorana fermions for two representative flux configurations. (a) The dispersions for the 3×3 for $K/J = 0$, which shows a gapped dispersion. (b)–(d) The Majorana dispersions for 4×4 supercell are shown for $K/J = 0.0$ in (b), $K/J = 0.01$ in (c), and $K/J = 0.175$ in (d). $K/J > 0$ opens a band gap across the zero energy. The adjacent right-hand panel shows the density of states (DoS) for all three cases. The **k** directions are given in the inset. The dispersions are shown only for $\epsilon(k) > 0$; redundant particle-hole symmetric $\epsilon(k) < 0$ are excluded.

The gap to the higher-energy bands is larger than that at $E = 0$. We denote the gap at $E = 0$ by Δ, while the bandwidth of the corresponding two low-energy bands is denoted by δ. The ratio δ/Δ, called the flatness ratio, measures the flatness of the low-energy bands, with $\delta/\Delta \to 0$ corresponding to complete flatness (i.e., all **k** points are degenerate) Fig. 3(d), while $\delta/\Delta \to \infty$ corresponds to point degeneracy, Fig. 3(b). K controls the band gap $\Delta(K)$, while the larger the length (d) of the $\mathbb{Z}_2$ flux pair, the smaller is δ, and typically δ scales allegorically as $\delta \sim 1/d^2$.

Increasing d while holding all other parameters constant elevates the sublattice dimension. In other words, it expands the dimension of the local Hilbert space C_I. This, in turn, enhances the level repulsion from the eliminated high-energy bands to the target low-energy bands. This repulsion is captured by the quantum metric $\mathcal{G}$ in the wave function description or by the superexchange or gauge potential (H') within our effective theory; see Fig. 3(c).

As K increases, we observe a fascinating topological phase transition, depicted in Fig. 5. Initially, the gap scales as $\Delta \sim K$ for $K \to 0$, before it reaches a maximum around $K \approx 0.06J$. This is an interesting point where the band gap varies minimally with K. With a further increase of K, Δ reduces and eventually vanishes entirely around $K \approx 0.175J$. Notably, the bandwidth (δ) also vanishes at this critical point, suggesting the formation of a completely flat band where both bands become degenerate across all **k** points. This results in an extensive degeneracy in the Hamiltonian. It is noteworthy that on either side of this flat band degeneracy, the system exhibits well-defined Chern bands with $C = \pm 1$ [88]. This observation suggests a unique type of topological phase transition characterized by the emergence of an extensive band degeneracy, which is different from the quintessential Dirac cone degeneracy at other topological phase transitions; see Sec. IV C.

B. Effective model and Majorana Wannier centers

We proceed by constructing an effective Hamiltonian H_{eff} to capture the behavior of the two low-energy bands ($\alpha = 1$, and $a = \pm$) and the localization of the corresponding Wannier orbitals $|\pm, \mathbf{R}\rangle$. Here, we focus on the supercell results for the $d = 4$ case for $K \neq 0$, i.e., a gapped system. We note that stabilizing a 4×4 flux configuration typically requires third nearest-neighbor hoppings [56,57], while still preserving the essential physics including Majorana band structure, flat bands, topology, and fractional Chern states, though these features may appear at different values of K. The construction of the effective band mirrors the example provided in Sec. III B, utilizing the same sets of nearest neighbors, except the $\mathbf{G}_{1,2}$ are different here. We expand the Hamiltonian up to several nearest neighbors, incorporating the coupling constants, and the specific values of the TB parameters are given in Appendix C 4. The fitting yields a near-perfect fit of the energy dispersions $\pm E(\mathbf{k})$ to the original supercell results;

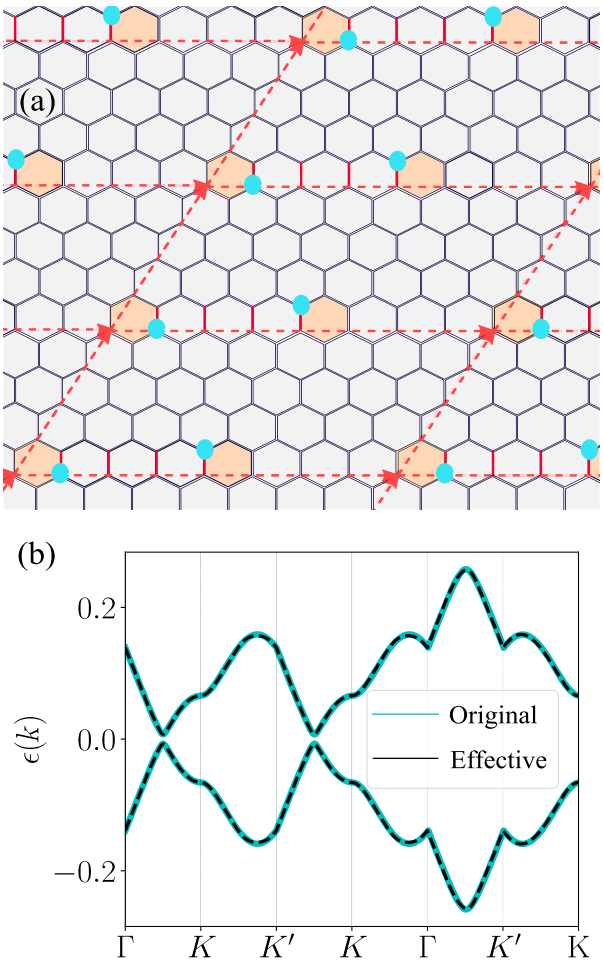


FIG. 4. (a) The locations of the Wannier centers (cyan color) are shown to be adjacent to the π-flux plaquettes for the 4×4 supercell. (b) The band structures from the original band structure and the effective Hamiltonian are shown for $K/J = 0.01$ on 4×4 configuration.

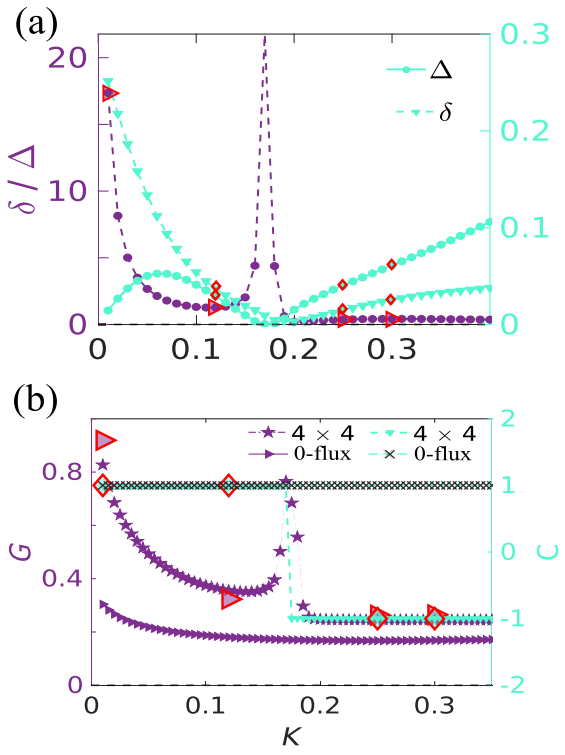


FIG. 5. (a) Band gap (Δ), bandwidth (δ), and the flatness ratio (δ/Δ) are plotted as a function of K from original model in Eq. (3) [verified values from the effective model in Eq. (18) are highlighted in red] for the 4×4 supercell. (b) Computed values of the quantum metric invariant (G) and Chern number (C) are plotted as a function of K and compared with zero-flux configuration. Two topological phase transitions are located here: at $K = 0$, we have a topological phase transition from trivial to nontrivial phase with Dirac cone degeneracy, and another one at $K \approx 0.175J$ between two nontrivial topologies with a flat band degeneracy whose dispersions are shown in Fig. 3(d).

see Fig. 4(b). For the fitting procedure, we use the WANNIER90 code [89]. A key advantage of using the WANNIER90 code is its ability to provide the real-space projection of the $w_{\pm,\mathbf{R}}(\mathbf{r})$, and their corresponding spread functions $\Delta\mathbf{r}_{\pm}$. Because of the nonzero Chern numbers of these flat bands, identifying their Wannier centers presents a challenge due to global gauge obstruction. In the effective theory, this gauge obstruction is evaded by choosing uniform flux W_S at all unit cells. The flux condition deduced in the effective Hamiltonian in Eq. (18) gives constraints on the fitting parameters. This method is discussed in Appendix C.

As anticipated, the Majorana Wannier orbitals $w_{\pm,\mathbf{R}}(\mathbf{r})$ are localized at the $\mathbb{Z}_2$ flux sites, as shown in Fig. 4(a). In fact, an isolated Majorana orbital with a $\mathbb{Z}_2$ flux makes a composite Majorana (zero-energy) Wannier orbital [43,54,90], and their periodic arrangements with finite nearest-neighbor tight-binding hopping strength produce dispersive bands. Within the original supercell, these two states were linked by the string operator that connects the $\mathbb{Z}_2$ flux pair. However, in effective theory, $w_{\pm,\mathbf{R}}(\mathbf{r})$ represents the two basis states of a unit cell. Since the effective gauge fields reside on the links connecting lattice sites, there is no gauge field directly coupling the two Majorana orbitals within a unit cell. Their coupling is not parametrized by the antisymmetric on-site interaction term $i\mathcal{K}_0 = K_0\sigma^z + K_0'\sigma^y$, where σ^μ matrices are defined in the $a = \pm$ Wannier orbital basis, as in the example case given in Sec. III B. Here, K_0 captures the on-site energy difference of the two orbitals, while K_0' describes the intraunit cell coupling between them. The remaining terms in Eq. (18) remain the same.

C. Chern number and quantum metric

This work suggests that the $\mathbb{Z}_2$ flux quantization condition within the supercell leads to similar properties as in the integer U(1) flux quantization condition in a magnetic Brillouin zone in the Thouless, Kohmoto, Nightingale, Den

Nijs (TKNN) theory for U(1) quantum Hall insulators [91]. Both mechanisms lead to a finite Chern number for each Majorana band, a characteristic that persists in both the full supercell Hamiltonian and the resulting effective theory.

Alternatively, we can interpret this behavior by parametrizing the eliminated states either as a geometry term in the wave function or as gauge fields within the Hamiltonian. A trivial topological space would correspond to a product state between the low-energy states and the eliminated states. Conversely, a nontrivial topology signifies entangled states between them. In the case of flat band geometry encountered here, a nontrivial topology necessarily arises.

To ensure consistency, we compute the Chern number for both cases. In the supercell case, we employ the projector $\mathcal{P}(\mathbf{k})$ to compute the Chern number (C) using Eq. (17). Similarly, for the effective Hamiltonian, C is obtained using its projector $\tilde{\mathcal{P}}(\mathbf{k}) = |\tilde{\mathbf{p}}, \mathbf{k}\rangle\langle\tilde{\mathbf{p}}, \mathbf{k}|$, where $|\tilde{\mathbf{p}}, \mathbf{k}\rangle$ are the eigenstates of $\mathcal{H}_{\text{eff}}(\mathbf{k})$. We present the results for the $d = 4$ case and compare them with the zero-flux ($d = 0$) scenario. Our calculations consistently reveal that the $K \neq 0$ case exhibits a Chern number of $C = +1$ for both $d = 0$ and $d = 4$ cases [for the $-E(\mathbf{k})$ band]. However, in the $d = 4$ supercell, a sharp transition from $C = +1$ to -1 occurs at the critical point $K = 0.175J$, where the band gap (Δ) closes and reopens. The underlying physics governing the Chern number transition obtained from the effective Hamiltonian $\mathcal{H}_{\text{eff}}(\mathbf{k})$ is analogous in which the uniform flux sector changes from $W_s = +1$ to $W_s = -1$. The transition is different from the gap closing and reopening at a single Dirac point: the involvement of the flat band at this transition point to a novel topological phase transition.

The influence of flat band physics and the geometry effect introduced by the eliminated high-energy states are effectively captured by the quantum metric [$\mathcal{G}(\mathbf{k})$] term in Eq. (10). The corresponding invariant (G) is defined in Eq. (16) and is plotted in Fig. 5(b) as a function of K [92]. As expected, the G value for the zero-flux configuration exhibits no distinguishing features, reinforcing the notion that G captures a distinct topological invariant arising from the projector, separate from the Chern number. In the supercell case, however, G displays an additional singularity at the gap-closing point of $K = 0.175J$. Interestingly, both G and the flatness ratio δ/Δ exhibit similar behavior. This suggests that the singularity in G is sensitive to the characteristics of the flat band, particularly the presence of extensive band degeneracy.

It is important to distinguish between the phase transition properties of interacting and noninteracting systems. In interacting theories, a second-order phase transition is characterized by the appearance of gapless collective modes and singular correlation functions. In contrast, in this noninteracting theory, an extensive degeneracy emerges at the flat bands. Here, the flat bands exhibit maximal entanglement with the eliminated high-energy bands, and consequently, we expect this unique phase transition feature to be reflected in the topological entanglement entropy [93–96].

A nonzero Chern number C signifies an obstacle in smoothly changing the wave function's phase [$\arg(w_{a,\mathbf{R}})$] throughout the material [97,98]. In contrast, a nonzero quantum metric G directly affects how "spread out" ($\Delta\mathbf{r}_a$) the wave function is [99,100]. More generally, $\mathcal{G}$ puts constraints on how different parts of the wave function are correlated, and $\Delta\mathbf{r}_a$ is a type of correlation function. In the effective Hamiltonian $\mathcal{H}_{\text{eff}}(\mathbf{k})$, the winding number of the wave function is determined by the complex phase of the off-diagonal term $\Delta_I(\mathbf{k}) + ih_s(\mathbf{k})$. $\Delta_R(\mathbf{k})$ acts like a Dirac mass term, which gives the inverse correlation length of the wave function, essentially defining its spread. At discrete Dirac points, all these terms simultaneously vanish at a single $\mathbf{k}$ point, while for the degenerate flat bands, they vanish at all $\mathbf{k}$ points. In our effective theory, $\Delta_{I,R}$ and h_S are assumed to be polynomials of Bloch phases $z_{\mathbf{R}}(\mathbf{k})$, which are a set of linearly independent basis functions. Consequently, a flat band arises when all the coefficients in these polynomials, i.e., the TB parameters $\mathcal{K}_i$, become zero.

D. Gauge-invariant mean-field theory for fractional Chern insulator

The interplay between $\mathcal{U}$ and $\mathcal{G}$ creates a promising platform for realizing fractional Chern insulating states through interactions [101–103]. The current understanding of fractional Chern insulating state primarily relies on numerical results [101–112]. In this section, we propose a mean-field theory that predicts the emergence of a fractional Chern number in Majorana bands.

We introduce a mean-field theory to split the Majorana flat bands by forming a density wave order state. A density wave state effectively folds the BZ into a reduced BZ, with the ordering vector $\mathbf{Q}$ defining the new reciprocal lattice vectors. The original Chern bands transform into a main band and folded (or shadow) bands within the reduced BZ. These bands share partial occupation density. This process leads to a fascinating consequence: A single, split Chern band becomes partially filled with a finite interacting gap separating it from another partially filled Chern band [101–103,113].

Here, we begin by verifying if the bands fulfill the essential criteria for an ideal "vortexable" band, a prerequisite for realizing a fractional Chern phase [65,107,114,115]. Interestingly, the low-energy Majorana bands in the supercell configurations fulfill those conditions: (i) uniform-in-$\mathbf{k}$ Berry curvature $U(\mathbf{k}) = \text{Tr}\mathcal{U}_{\mu\nu}(\mathbf{k})$ and (ii) the trace condition $G(\mathbf{k}) = \frac{1}{2}\sum_\mu \text{Tr}\mathcal{G}_{\mu\mu}(\mathbf{k}) \simeq U(\mathbf{k})$, $\forall$ $\mathbf{k}$ point. Another quantity that measures how good is a flat band is called the flatness ratio (δ/Δ), where δ is the bandwidth of each flat band, and Δ is the band gap between the two flat bands under consideration. When δ/Δ is less,

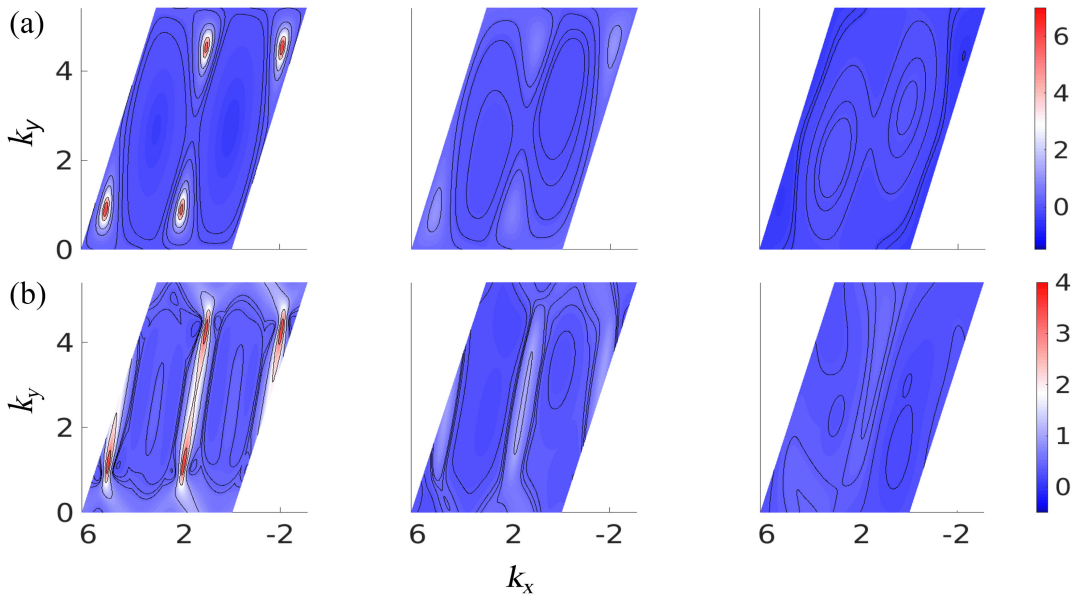


FIG. 6. We plot (a) the Berry curvature $G(\mathbf{k})$ and (b) the difference $G(\mathbf{k}) - \mathbf{U}(\mathbf{k})$ from the trace condition (ii) in the first Brillouin zone. The plots in each column correspond to different K values of 0.035, 0.12, and 0.22, from left to right.

as shown in Fig. 5(a) for the 4×4 supercell, the conditions for ideal Chern bands are satisfied more accurately. Figure 6(a) shows $U(\mathbf{k})$ and Fig. 6(b) gives the difference $G(\mathbf{k}) - U(\mathbf{k})$ in (ii) at three different K values, 0.035, 0.12, and 0.22 from left to right. δ/Δ decreases with increasing K, and $U(\mathbf{k})$ becomes more uniform. The same is true for the trace condition in (ii); i.e., the difference $G(\mathbf{k}) - U(\mathbf{k})$ is much less with increasing K.

Having established that the Chern Majorana bands in the supercell settings are prone to fractionalization, we now include an interaction term within the effective Hamiltonian H_{eff} in Eq. (14), or more specifically in Eq. (18) for the case of 2×2 honeycomb lattice. Interestingly, a $\mathbb{Z}_2$ "electric field" operator introduced below Eq. (2) mediates a quartic Majorana interaction in the honeycomb lattice with three nearest neighbors [38,57]. The corresponding operator for the Wannier orbitals, in general, reads as $X_{\mathbf{R}} = \prod_{\{\mathbf{R}^{(1)}\} \in d_1} \mathcal{U}_{\mathbf{R},\mathbf{R}^{(1)}}$, where it is reminded that $\mathbf{R}^{(1)}$ is a set of first nearest-neighbor sites containing d_1 elements with respect to the $\mathbf{R}$ site. $X_{\mathbf{R}}$ is a gauge-dependent operator, and it couples to all the Majoranas sitting at $\mathbf{R}$ and $\mathbf{R}^{(1)}$, which then becomes gauge invariant. In the original Kitaev model with the small magnetic field, it was shown that such a term arises in the same third-order perturbation term as in Eq. (2) and has the same coupling constant of iK. Here in the effective model, such a term can arise from the multiple virtual hoppings to the eliminated states and can be obtained by higher-order polynomial fittings along the line done for the quadratic term in Eq. (7). We consider a general coupling term of $i\mathcal{K}_1'$ and write the interaction term on a honeycomb lattice and $a = \pm$ particle-hole Majorana pair in a single $\alpha = 1$ orbital state as

$$H_{\text{int}} = -i\mathcal{K}_1' \sum_{\mathbf{R},a,a'=\pm} i u_{\mathbf{R},\mathbf{R}_1^{(1)}} u_{\mathbf{R},\mathbf{R}_2^{(1)}} u_{\mathbf{R},\mathbf{R}_3^{(1)}} \times c_{a,\mathbf{R}} c_{a',\mathbf{R}_1^{(1)}} c_{a',\mathbf{R}_2^{(1)}} c_{a',\mathbf{R}_3^{(1)}}. \tag{20}$$

Consistent with Elitzur's theorem [116], we can write down two gauge-invariant mean-field order parameters, defined as follows:

$$\Omega_1 = \frac{i\mathcal{K}_1'}{3} \sum_{i=1}^{3} \langle u_{\mathbf{R},\mathbf{R}_i^{(1)}} c_{a,\mathbf{R}} c_{a',\mathbf{R}_i^{(i)}} \rangle, \tag{21}$$

$$\Omega_2 = -\frac{i\mathcal{K}_1'}{3} \sum_{i \neq j=1}^{3} \langle u_{\mathbf{R}_i^{(1)},\mathbf{R}_j^{(1)}} c_{a',\mathbf{R}_i^{(1)}} c_{a',\mathbf{R}_j^{(1)}} \rangle. \tag{22}$$

Here, the expectation value is self-consistently evaluated within the mean-field ground state. We have also assumed the order parameters $\Omega_{1,2}$ to be independent of $\mathbf{R}$ (uniform phase), and hence, it is dropped from the lhs of the above equation. Both order parameters involve two Majorana operators, and the gauge field links them so that the order parameter remains gauge invariant. The resultant mean-field interaction (gauge-invariant) Hamiltonian becomes

$$H_{\text{int}}^{(\text{MF})} = i\Omega_2 \sum_{\mathbf{R},i,a \neq a'} u_{\mathbf{R},\mathbf{R}_i^{(1)}} c_{a,\mathbf{R}} c_{a',\mathbf{R}_i^{(1)}} + i\Omega_1 \sum_{\mathbf{R},i \neq j,a'} u_{\mathbf{R}_i^{(1)},\mathbf{R}_j^{(1)}} c_{a',\mathbf{R}_i^{(1)}} c_{a',\mathbf{R}_j^{(1)}}, \tag{23}$$

In the second term in Eq. (22) and the first term in Eq. (23), we have implemented the relation $u_{\mathbf{R}_i^{(1)},\mathbf{R}_j^{(1)}} = -u_{\mathbf{R},\mathbf{R}_i^{(1)}} u_{\mathbf{R},\mathbf{R}_j^{(1)}}$. In the Fourier space, we assume $\Omega_{1,2}$

breaks the translational symmetry to a staggered density wave state at a fixed wave vector $\mathbf{Q}$ such that $\Omega_1(\mathbf{Q}) = \sum_{\mathbf{R}_i - \mathbf{R}_j^{(1)}} \Omega_1 e^{i\mathbf{Q}\cdot(\mathbf{R}_i - \mathbf{R}_j^{(1)})}$ and $\Omega_2(\mathbf{Q}) = \sum_{\mathbf{R} - \mathbf{R}_j^{(1)}} \Omega_2 e^{i\mathbf{Q}\cdot(\mathbf{R} - \mathbf{R}_j^{(1)})}$. While the above gauge-invariant mean-field theory admits various generalizations, we focus on a simpler case here to illustrate the emergence of partially filled Chern bands within this framework.

Adding $H_{\text{int}}^{(\text{MF})}$ to the effective Hamiltonian H_{eff} in Eq. (18), we can express the matrix form of the Hamiltonian in the spinor $(c_+(\mathbf{k})\, c_-(\mathbf{k})\, c_+(\mathbf{k}+\mathbf{Q})\, c_-(\mathbf{k}+\mathbf{Q}))^T$ for the $\alpha = 1$ band as

$$\mathcal{H}_{\text{MF}}(\mathbf{k}) = \begin{pmatrix} \mathcal{H}_{\text{eff}}(\mathbf{k}) & i\Omega(\mathbf{Q}) \\ \text{H.c.} & \mathcal{H}_{\text{eff}}(\mathbf{k}+\mathbf{Q}) \end{pmatrix},$$
$$\Omega(\mathbf{Q}) = \begin{pmatrix} \Omega_1(\mathbf{Q}) & \Omega_2(\mathbf{Q}) \\ \Omega_2^*(\mathbf{Q}) & \Omega_1^*(\mathbf{Q}) \end{pmatrix}. \tag{24}$$

The above form of $\Omega(\mathbf{Q})$ maintains the particle-hole symmetry of the Hamiltonian. The eigenvectors of the mean-field Hamiltonian in Eq. (24) are used in Eqs. (21) and (22) to calculate these order parameters self-consistently.

We test our results for a simpler commensurate density wave order for $\mathbf{Q} = \mathbf{G}_2/2$, and $\Omega_1 = 0.01$, $\Omega_2 = 0.015$ with $K = 0.12$. The corresponding energy eigenvalues of $\mathcal{H}_{\text{MF}}(\mathbf{k})$ split the particle-hole symmetric eigenvalues $\pm E_{\mathbf{k}}$ into four bands with a finite gap between all of them. The Chern number of each band now corresponds to $C_n = \sum_{\mathbf{k}\in\text{RBZ}} \sum_a \mathcal{V}_{na}^\dagger(\mathbf{k}) \mathcal{V}_{na}(\mathbf{k}) \text{Tr}_a \mathcal{U}_{12}(\mathbf{k})$, where $\mathcal{V}$ corresponds to the eigenvectors of $\mathcal{H}_{\text{MF}}$, and Tr_a corresponds to the trace operation with the $a = \pm$ eigenvector on the Berry curvature given in Eq. (11). RBZ corresponds to the reduced BZ in the density wave state. The obtained values of the Chern number for all four bands are $C = 0.129$, 0.505, -0.873, and -0.4.

V. SUMMARY AND OUTLOOK

Our work has two major advancements: (i) We construct a lattice model for generalized fractional orbitals hopping under tailored gauge potentials and (ii) we apply this model to Majorana fermions in the flux-crystalline phase of the Kitaev model, exploring interaction effects and fractional Chern states via a mean-field approach.

In the first part of the model development, we have kept the theory general for any fractional quasiparticles. This approach is extendable to other fractional quasiparticles and represents a significant step forward in addressing long-standing challenges like Wannier obstructions. The key idea lies in starting with a well-defined Wannier orbital ansatz—a topologically trivial product state—and then sculpting the desired topology and quantum metric through an effective Hamiltonian that incorporates a projector and a variational geometric potential. Secondly, we derive the tight-binding gauge fields from the quadratic terms in the Taylor expansion [Eqs. (6) and (7)] and the interaction terms from the quartic terms [Eq. (20)]. This elegantly transfers the constraints imposed by the projection operator on Wannier orbital correlations to the correlations encoded within the emergent geometric potential. This makes the formalism general and applicable to generic fractional states.

We applied our framework to Majorana orbitals in the flux-crystalline phase of the Kitaev model, focusing on their interaction effects and fractional Chern states through a mean-field method. While the full dispersion of Majorana bands in various flux superlattices of the Kitaev model has been extensively studied [55,56,61–64], a crucial missing piece has been a proper tight-binding description, including the quantum metric and the emergence of fractional Chern states. Our work fills this gap with several key advancements. (a) We constructed a TB model for Majorana orbitals by introducing a geometric potential—arising from virtual hopping to eliminate high-energy states—and systematically derived both quadratic and quartic interactions mediated by this potential. We also elucidated the conditions under which these potentials manifest as a $\mathbb{Z}_2$ gauge field and quantum metric, ensuring flux preservation and consistency with the original supercell Hamiltonian. (b) We then analyzed the evolution of the Berry curvature and quantum metric of the effective theory as flat bands emerge with increasing nearest-neighbor hopping. Strikingly, we uncovered a novel critical point where the quantum metric diverges, signaling a phase transition between $C = \pm 1$ phases within the same band. This hallmark of flat bands with extensive degeneracy suggests, even at the noninteracting level, a state of maximal entanglement between low- and high-energy states. (c) Finally, building on the existence of flat bands with a divergent quantum metric, we developed a mean-field theory to describe a gauge-invariant Majorana density wave order. The resulting split Chern bands enable partial filling with a gapped spectrum relative to other Majorana bands. This mean-field theory provides an analytically tractable framework for understanding fractional Chern insulator states in these fascinating systems.

The proposals for attaining control over the creation or annihilation of $\mathbb{Z}_2$ fluxes are reviewed first. Theoretically, approximate studies predict the existence of flux superlattices in the Kitaev model with further nearest-neighbor hoppings [55] and also with the applied magnetic field [62]. An unbiased density matrix renormalisation group (DMRG) study of the Kitaev model with external magnetic fields provided evidence for the emergence of various flux superlattices [19]. In general, the Heisenberg model on some frustrated lattices can host various flux crystals predicted by projective symmetry group analysis, giving rise to diverse spin-liquid phases [117–119]. Experimentally, creating and

stabilizing these flux superlattices is challenging. In recent times, it has been theoretically proposed in Ref. [120] that the local modulation of exchange interactions by introducing Dzyaloshinskii-Moriya interactions flips the sign of local bond interactions. That produces a $\mathbb{Z}_2$ flux pair. Further desired configurations are obtained by creating or annihilating the sequence of pairs in neighboring plaquettes. In general, superconducting quantum interference device (SQUID) microscopy is helpful in experimentally visualizing these vortex networks [121].

This work centers on constructing a gauge-field-mediated TB model for fractional particles. Since fractional or entangled excitations do not exist by themselves, their combinations must produce electronic states. Alternatively, one can view these fractional particles as residing within a medium of gauge fields, either confined or deconfined. Our focus is twofold: understanding the origin of these gauge fields and establishing a systematic framework for their parametrization within a TB model. The emergence of such gauge fields comes from the projection operation used to eliminate high-energy states. This operation effectively imposes constraints, leading to restricted dynamics and correlation functions pertaining to fractional particles. These constrained dynamics can give rise to more phenomena such as a distinct type of quantum glass [19], or deconfined critically [122,123], or extensive degeneracy in the formation of flat bands, leading to novel topological critically in the noninteracting theory as observed here.

Our approach deviates from conventional methods by introducing a gauge potential directly within the Hamiltonian through a superexchange mechanism. This mechanism gives rise to gauge-mediated tight-binding hoppings arising from the antisymmetric part of the superexchange potential. Notably, an additional constraint can be readily incorporated to ensure flux preservation and topology without worrying about the maximal localization of the Wannier orbitals. The detailed constructions provided in Sec. III apply to a general SU(N) gauge field, $\mathcal{U}$, and its corresponding fractional particle. In this specific work, we have inserted the $\mathbb{Z}_2$ valuedness of the $\mathcal{U}$ operators toward the end and in the particle-hole symmetry of $\mathcal{H}_{\text{eff}}$, which ensures real Majorana states in real space. Therefore, it will be rather straightforward to generalize the TB theory to the SU(N) gauge field coupled to other fractional particles. These effective models of fractional particles are useful in constructing more precise spectroscopic probes for their detection.

Our analysis reveals an interacting critical point within the theory as a function of the second nearest-neighbor hopping strength (K). At this critical point, the quantum metric diverges, and the Chern number exhibits a transition between $+1$ and -1. This signifies a potential singularity in the entanglement entropy spectrum, where the entanglement is maximal between the low-energy and the eliminated high-energy states. Quantifying this entanglement spectrum in terms of gauge-mediated TB parameters remains an intriguing challenge for future investigations.

Finally, leveraging the insights from the effective Hamiltonian, we propose a mean-field theory for a gauge-invariant Majorana density wave order. In conventional gauge theories, the mean-field order parameter is subject to an additional constraint arising from the requirement of gauge invariance. This constraint often presents significant challenges within the geometric framework, leading to a reliance on numerical methods for studying fractional Chern insulator states. Our effective Hamiltonian, however, allows us to derive a self-consistent mean-field theory for Majorana fermions. This method paves the way for future investigations into more exotic interaction effects within both $\mathbb{Z}_2$ and SU(N) gauge theories.

ACKNOWLEDGMENTS

K. B. Y. thanks Partha Sarathi Rana for his help with the WANNIER90 code. The work is supported by research funding from the S. E. R. B. Department of Science and Technology, India, under Core Research Grant (CRG) Grant No. CRG/2022/00341m and under I. R. H. P. A Grant No. IPA/2020/000034. We also acknowledge the computational facility at S. E. R. C. Param Pravega under National Supercomputing Mission (NSM) Grant No. DST/NSM/R&D HPC Applications/2021/39.

APPENDIX A: MATRIX ELEMENTS OF THE SUPERCELL HAMILTONIAN

Here, we explicitly give the matrix elements of the $2N \times 2N$ matrices $\mathcal{H}_{IJ}$ as

$$\mathcal{T}_{II} = \begin{pmatrix} 0 & Ju_{1,2} & Ku_{1,2}u_{2,3} & 0 & \dots & 0 & 0 \\ -Ju_{1,2} & 0 & Ju_{2,3} & Ku_{2,3}u_{3,4} & \dots & 0 & 0 \\ -Ku_{1,2}u_{2,3} & -Ju_{2,3} & 0 & Ju_{3,4} & \dots & 0 & 0 \\ 0 & -Ku_{2,3}u_{3,4} & -Ju_{3,4} & 0 & \dots & 0 & 0 \\ \vdots & \vdots & \vdots & \vdots & \ddots & 0 & Ju_{2N-1,2N} \\ 0 & 0 & 0 & 0 & 0 & -Ju_{2N-1,2N} & 0 \end{pmatrix}, \tag{A1}$$

and

$$\mathcal{T}_{IJ} = \begin{pmatrix} 0 & 0 & 0 & \dots & 0 \\ \vdots & \vdots & \vdots & \ddots & \vdots \\ 0 & 0 & 0 & \dots & 0 \\ Ku_{2N-1,2N}u_{2N,1} & 0 & 0 & \dots & 0 \\ Ju_{2N,1} & Ku_{2N,1}u_{12} & 0 & \dots & 0 \end{pmatrix}. \tag{A2}$$

The matrix elements in the momentum space become

$$\mathcal{H}(\mathbf{k}) = i\mathcal{T}_{II} + \begin{pmatrix} 0 & 0 & 0 & \dots & 0 & \mathcal{K}_{1,2N-1}(\mathbf{k}) & \mathcal{J}_{1,2N}(\mathbf{k}) \\ 0 & 0 & 0 & \dots & 0 & 0 & \mathcal{K}_{2,2N}(\mathbf{k}) \\ 0 & 0 & 0 & \dots & 0 & 0 & 0 \\ \vdots & \vdots & \vdots & \ddots & \vdots & \vdots & \vdots \\ 0 & 0 & 0 & \dots & 0 & 0 & 0 \\ \mathcal{K}^*_{1,2N-1}(\mathbf{k}) & 0 & 0 & \dots & 0 & 0 & 0 \\ \mathcal{J}^*_{1,2N}(\mathbf{k}) & \mathcal{K}^*_{2,2N}(\mathbf{k}) & 0 & \dots & 0 & 0 & 0 \end{pmatrix}, \tag{A3}$$

where $\mathcal{K}_{1,2N-1}(\mathbf{k}) = iKu_{2N-1,2N}u_{2N,1}e^{-i\mathbf{k}\cdot(\mathbf{R}_1-\mathbf{R}_{2N-1})}$, $\mathcal{J}_{1,2N}(\mathbf{k}) = iJu_{2N,1}e^{i\mathbf{k}\cdot(\mathbf{R}_1-\mathbf{R}_{2N})}$, $\mathcal{K}_{2,2N}(\mathbf{k}) = iKu_{2N,1}u_{1,2}e^{-i\mathbf{k}\cdot(\mathbf{R}_2-\mathbf{R}_{2N})}$.

APPENDIX B: MATRIX ELEMENTS OF THE TIGHT-BINDING MODEL

To ensure the Majorana operators are well defined, and the corresponding complex fermion operators recover the U(1) gauge fields, we transform the Hamiltonian on a complex fermion basis. For each Majorana pair orbitals, $a = \pm$, the corresponding particle-hole pairs of complex fermions at different momenta are related by

$$|\alpha, a, \mathbf{k}\rangle = +e^{i\phi_{\alpha,a}}|\alpha, -, -\mathbf{k}\rangle_F + e^{-i\phi_{\alpha,a}}|\alpha, +, \mathbf{k}\rangle_F. \tag{B1}$$

where $\phi_{\alpha,+} = 0$ and $\phi_{\alpha,-} = \pi/2$. $|\alpha, \pm, \mathbf{k}\rangle_F$ are the complex fermionic hole and particle excitation states defined as $|\alpha, +, \mathbf{k}\rangle_F = f_{\alpha,\mathbf{k}}|G\rangle$ and $|\alpha, -, \mathbf{k}\rangle_F = f^\dagger_{\alpha,\mathbf{k}}|G\rangle$ with $f_{\alpha,\mathbf{k}}$ and $f^\dagger_{\alpha,\mathbf{k}}$ corresponding annihilation and creation operators of complex fermions from some grand canonical ensemble state $|G\rangle$. It is easy to see that the corresponding Majorana and complex fermion operators are local in real space as $|\alpha, a, \mathbf{R}\rangle = e^{i\phi_{\alpha,a}}|\alpha, -, \mathbf{R}\rangle_c + e^{-i\phi_{\alpha,a}}|\alpha, +, \mathbf{R}\rangle_c$. Note that $|\alpha, a, \mathbf{R}\rangle$ are the physical Majorana states in real space, whereas complex fermions correspond to physical states in both real and momentum spaces. There is an inherent gauge obstruction between the two Majorana orbitals by a phase difference of $\phi_\alpha = \phi_{\alpha,+} - \phi_{\alpha,-}$. We have kept this phase difference to be orbital independent, but it can be generalized to be orbital dependent, which may commence interesting properties.

We construct a $2P$-dimensional Majorana spinor as $|\alpha, +, \mathbf{k}\rangle \oplus |\alpha, -, \mathbf{k}\rangle$ and complex fermionic particle-hole symmetric Nambu spinor $|\alpha, +, \mathbf{k}\rangle_F \oplus |\alpha, -, -\mathbf{k}\rangle_F$. The transformation between them is defined by the unitary operator:

$$\mathcal{S} = \frac{1}{2}\begin{pmatrix} 1 & i \\ 1 & -i \end{pmatrix} \otimes I_{P\times P}. \tag{B2}$$

The Majorana Hamiltonian given in the main text is written generally as

$$H_{\text{eff}} = h_A \otimes \mathcal{I}_{2\times 2} + \begin{pmatrix} \Delta_R & \Delta_I + ih_S \\ \text{H.c} & -\Delta_R \end{pmatrix}, \tag{B3}$$

where $\mathbf{k}$ dependence in all variables is kept implicit. Here $h_{S/A}(\mathbf{k}) = h(\mathbf{k}) \pm h^T(-\mathbf{k})$, and $\Delta(\mathbf{k}) = \Delta_R(\mathbf{k}) + i\Delta_I(\mathbf{k})$. Then, transforming this Hamiltonian to the complex fermion basis gives

$$H^{(\text{F})}_{\text{eff}} = \frac{1}{4}\mathcal{S}H_{\text{eff}}(\mathbf{k})\mathcal{S}^\dagger = \begin{pmatrix} h(\mathbf{k}) & \Delta(\mathbf{k}) \\ \Delta^\dagger(\mathbf{k}) & -h^T(-\mathbf{k}) \end{pmatrix}. \tag{B4}$$

This is a typical Bogoluybov–de Gennes Hamiltonian in the particle-hole basis, where $h_\mathbf{k}$ is a $P \times P$ Hamiltonian for complex-fermions hopping, and $\Delta(\mathbf{k})$ is the $P \times P$ matrix consisting of superconducting pairings of the complex fermions.

The explicit form of the matrix elements of Eq. (B3) can be written as

$$(\Delta_R)_{\alpha,\alpha'}(\mathbf{k}) = \sum_{p,p'=1}^{P} \langle \alpha,+,\mathbf{k}|p,+,\mathbf{k}\rangle\langle p,+,\mathbf{k}|(H+H')|p',+,\mathbf{k}\rangle\langle p',+,\mathbf{k}|\alpha',+,\mathbf{k}\rangle, \tag{B5}$$

$$(\Delta_I + iH_S)_{\alpha,\alpha'}(\mathbf{k}) = \sum_{p,p'=1}^{P} \langle \alpha,+,\mathbf{k}|p,+,\mathbf{k}\rangle\langle p,+,\mathbf{k}|(H+H')|p',-,\mathbf{k}\rangle\langle p',-,\mathbf{k}|\alpha',-,\mathbf{k}\rangle. \tag{B6}$$

Because of particle-hole symmetry, $|p,+,\mathbf{k}\rangle$ states give $|\alpha,+,\mathbf{k}\rangle$ Majorana orbital, while $|p,-,\mathbf{k}\rangle$ states give $|\alpha,-,\mathbf{k}\rangle$ orbital, respectively. We define $(U_\pm)_{\alpha,p} = \langle \alpha,\pm,\mathbf{k}|p,\pm,\mathbf{k}\rangle$ a $P\times P$ overlap matrix which consists of the probability amplitudes of the particle-hole symmetric eigenstates of the full Hamiltonian $|p,\pm,\mathbf{k}\rangle$ to the effective Majorana orbital states. Note that U is not a unitary operator as $|p,\pm,\mathbf{k}\rangle$ states are incomplete. We denote the matric elements of H are $(\mathcal{D}_\pm)_{p,p'}(\mathbf{k}) = \langle p,\pm,\mathbf{k}|H|p',\pm,\mathbf{k}\rangle = \pm E_p(\mathbf{k})\delta_{p,p'}$. The matrix elements H' can be written in second-order perturbation theory with respect to some gauge interaction or superexchange potential V that makes the transition from the $\mathcal{P}$ to the $\mathcal{Q}$ states as

$$\begin{aligned}(\mathbf{H}'_{aa'})_{p,p'} &= \langle p,a,\mathbf{k}|H'|p',a',\mathbf{k}\rangle \\ &= \frac{1}{2}\sum_{q,q'\in\mathcal{Q}} (V_a)_{pq}(V_{a'})_{q'p'}\left[\frac{\mathrm{sgn}(a)}{E_p - E_q} - \frac{\mathrm{sgn}(a')}{E_{q'} - E_{p'}}\right] \\ &\quad + \cdots.\end{aligned} \tag{B7}$$

Here $q\in\mathcal{Q}_\pm = \mathcal{I} - \mathcal{P}_\pm$ states are the particle-hole pairs outside the subspace of our interest. $(V_\pm)_{pq} = \langle p,\pm,\mathbf{k}|V|q,\pm,\mathbf{k}\rangle$ is the tunneling amplitude between the two eigenstates, our fitting parameters. $|p,\pm,\mathbf{k}\rangle$ are the eigenstates of H and hence are particle-hole symmetric. Interestingly, H' is not particle-hole symmetric in the $|p,\pm,\mathbf{k}\rangle$ as it allows for transition between the particle-hole symmetric states in Eq. (B6), but its matrix elements must be particle-hole symmetric in the $|\alpha,\pm,\mathbf{k}\rangle$ states, by construction. If C is the particle-hole symmetric operator in the $|\alpha,\pm,\mathbf{k}\rangle$ basis, defined as $|\alpha,+,\mathbf{k}\rangle = \mathsf{C}|\alpha,-,\mathbf{k}\rangle$, the matrix elements transform as $\mathsf{C}\mathcal{D}_+(\mathbf{k})\mathsf{C}^{-1} = -\mathcal{D}_-(\mathbf{k})$, $\mathsf{C}\mathcal{H}'_{++}(\mathbf{k})\mathsf{C}^{-1} = -\mathcal{H}'_{--}(\mathbf{k})$, and $\mathsf{C}\mathcal{H}'_{+-}(\mathbf{k})\mathsf{C}^{-1} = -\mathcal{H}'_{-+}(\mathbf{k})$. Substituting them in Eqs. (B5) and (B6) we get $\Delta_R = -U_+(\mathcal{D}_+ + \mathcal{H}'_{++})U_+^{-1} = -U_-(\mathcal{D}_- + \mathcal{H}'_{--})U_-^{-1}$ and $(\Delta_I + i\mathcal{H}_S) = U_+\mathcal{H}'_{+-}U_-^{-1} = -U_-\mathcal{H}'_{-+}U_+^{-1}$, $\forall\ \mathbf{k}$.

APPENDIX C: NUMERICAL FITTING PROCEDURE

1. Gauge obstruction and spread function of Wannier Majorana states

Here, we address the issue of the gauge obstruction for Wannier orbitals of the electrons and how they transcend into the Wannier orbitals of fractional particles. Fixing a smooth global gauge for all Wannier orbitals of electrons within a unit cell can be hindered by several factors. Below, we discuss several such cases and their corresponding remedies.

(a) Topological insulators. In topological insulators, band inversion between two Wannier orbitals obstructs a global momentum space gauge. Here, the Wannier orbitals differ by a well-defined local gauge connection, reflecting the nontrivial topology. For example, while a Chern number of 1 requires a band inversion within the Brillouin zone, its specific location can be shifted without affecting the overall topology (movable gauge obstruction). As discussed in Refs. [23,124–131], this can be addressed by defining an appropriate gauge-fixing matrix.

(b) Gapless points. If a gapless point arises from a symmetry-protected degeneracy between two bands, it may not be readily movable (unless it is a gauge theory) [83,132,133]. This can be tackled by expressing the Wannier orbital states as superpositions within the degenerate manifold and carefully handling the singular point in the expansion coefficient (unitary matrix).

(c) Flat bands. Constructing Wannier orbitals becomes challenging for specific flat bands, particularly when they exhibit degeneracy with another band. In such cases, a complete set of localized compact Wannier orbitals may not be achievable. Instead, a combination of compact localized states and extended states might be necessary to form a complete basis set [74,75,134–140].

(d) Atomically obstructed insulators. This recently discovered class of (trivial or fragile) topological insulators presents a unique challenge [141–144]. Here, each of the multiple Wannier orbitals must individually possess a sufficiently small spread function ($\Delta\mathbf{r}$) such that their combined spread stays confined within a unit cell.

Can the aforementioned challenges be entirely overcome using Wannier orbitals for fractional particles within a gauge theory framework? The fractional particles of interest here arise from the superposition states of the original complex matter fermions. The fractional particles exhibit a physical separation in real space due to emergent local

gauge fields and/or topology. Their physical separation is linked by the gauge fields such as W_p, X_v, and $\mathcal{U}_{ij}$. For example, in the present case, the two Majorana orbitals are pinned at the two π-flux pairs that are separated by a distance d. Therefore, in analogy with the atomically obstructed orbitals, the spread function ($\Delta\mathbf{r}$) associated with each Majorana Wannier orbital must be less than $d/2$ if there exists a finite trivial gap between the two Majorana bands. For the gapless case, $\Delta\mathbf{r} \sim d/2$, whereas in a topologically nontrivial case, $\Delta\mathbf{r} > d/2$ such that the two Majorana Wannier orbitals overlap within the unit cell, and an intraunit-cell gauge field between the two orbitals contains a winding or knot to produce the topological invariant.

The gauge obstruction is incorporated within the eigenstates of the full Hamiltonian $|\mathbf{p},\mathbf{k}\rangle$ before fractionalizing them in the orbital states. This is done as in the standard method outlined in Ref. [24]. The procedure has two steps. First, we allow a unitary transformation $B(\mathbf{k})$ to the eigenstates as $|\tilde{\mathbf{p}},\mathbf{k}\rangle = \sum_p B_{\tilde{\mathbf{p}},\mathbf{p}}(\mathbf{k})|\mathbf{p},\mathbf{k}\rangle$—which incorporates the singular gauge that needs to be added or subtracted from the global gauge. Next, we fix the gauge on the rotated states $|\tilde{\mathbf{p}},\mathbf{k}\rangle$ between the two nearest momenta differ by the grid size of $\delta\mathbf{k} = 2\pi/L$, where L is the sample length. It turns out the spread function $\Delta\mathbf{r} = \sum_{\tilde{\mathbf{p}}}\langle\mathbf{r}^2\rangle_{\tilde{\mathbf{p}}} - \langle\mathbf{r}\rangle^2_{\tilde{\mathbf{p}}}$ is related to the overall matrix,

$$M_{\tilde{\mathbf{p}},\tilde{\mathbf{p}}'}(\mathbf{k},\mathbf{k}+\delta\mathbf{k}) = \frac{1}{\sqrt{2N}}\sum_i \sum_{\mathbf{p},\mathbf{p}'} B^\dagger_{\mathbf{p},\tilde{\mathbf{p}}}(\mathbf{k})\Gamma^\dagger_{i,\mathbf{p}}(\mathbf{k})\bar{z}_{\mathbf{t}_i}(\delta\mathbf{k}) \times \Gamma_{\mathbf{p}',i}(\mathbf{k}+\delta\mathbf{k})B_{\tilde{\mathbf{p}}',\mathbf{p}'}(\mathbf{k}+\delta\mathbf{k}), \quad \text{(C1)}$$

where $\mathbf{t}_i$ are the positions of the original $2N$ Majorana sublattices in the full Hamiltonian within the $\mathbf{R}$ supercell. Γ is the unitary matrix consisting of the eigenvector of the full Hamiltonian defined in Sec. II. $\mathbf{R}_{\boldsymbol{\alpha}}$ is the position of the α sublattice within the supercell, and we sum over all $\mathbf{R}$ in the entire lattice. In the main text, we work with the $|\tilde{\mathbf{p}},\mathbf{k}\rangle$ after the gauge fixing, which we continue to denote by $|\mathbf{p},\mathbf{k}\rangle$ for simplicity in notation.

2. Completeness of the Wannier Majorana states

In the above description, the $|\alpha,\pm,\mathbf{k}\rangle$ are defined to be the orthonormal, complete Wannier states of the effective $2P\times 2P$ Hamiltonian, $|p,\pm,\mathbf{k}\rangle$ are the low-energy eigenstates of our interest of the full Hamiltonian which are orthonormal but not complete. Our numerical procedure follows two steps. First, we construct $|\alpha,\pm,\mathbf{k}\rangle$ states iteratively and then use $\mathcal{K}_n$ as fitting parameters to find the corresponding energies $\pm E_p(\mathbf{k})$ subject to the flux conservation constraint. The procedure followed is the same as Ref. [23] and implemented in the WANNIER90 package.

We assume $|\alpha,\pm,\mathbf{k}\rangle_t$ as some trial nonorthogogonal complete Wannier states related to the $|p,\pm,\mathbf{k}\rangle$ states by an overall matrix $(U^{(t)}_\pm)_{p,\alpha}(\mathbf{k}) = \langle p,\pm,\mathbf{k}|\alpha,\pm,\mathbf{k}\rangle_t$. Note that $U^{(t)}_\pm$ are not the same as the desired overlap matrix $U_\pm$ defined below Eq. (B6) and we want to find a relation between them. To orthonormalize $|\alpha,\pm,\mathbf{k}\rangle_t$ we define their overlap matrix:

$$\begin{aligned}(S_\pm)_{\alpha\alpha'}(\mathbf{k}) &= \sum_{pp'}(U^{(t)\dagger}_\pm)_{\alpha,p}(\mathbf{k})(U^{(t)}_\pm)_{p',\alpha'}(\mathbf{k})\langle p,\pm,\mathbf{k}|p',\pm,\mathbf{k}\rangle \\ &= (U^{(t)\dagger}_\pm U^{(t)}_\pm)_{\alpha\alpha'}.\end{aligned}$$

Then the orthonormal Wannier states are defined as $|\alpha,\pm,\mathbf{k}\rangle = \sum_{\alpha'}(S^{-1/2}_\pm)_{\alpha\alpha'}(\mathbf{k})|\alpha',\pm,\mathbf{k}\rangle$. Then it is easy to show that the overlap matrix is defined as $U_\pm = U^{(t)}_\pm S^{-1/2}_\pm$, $\forall\ \mathbf{k}$. For the method to work, i.e., the Wannier orbitals to be smooth in the momentum space, the overall matrix $U^{(t)}_\pm$ must be nonsingular. This is often not the case for topological insulators, atomically obstructed insulators, or flat bands with singular compact orbitals. For removable singularity, the procedure works well as described in Refs. [74,83,124,126]. Note that we do not need separate trial functions for the $\pm$ states as they are related by the particle-hole symmetry $\mathcal{C}$.

3. Choosing the trial wave function

How do we efficiently guess the trial Wannier states $|\alpha,\pm,\mathbf{k}\rangle_t$? We follow the procedure outlined in Ref. [126] for complex fermions and make necessary modifications. Because we have the eigenvalues and eigenvectors of the full Hamiltonian H in the supercell, we study first where our interested eigenvectors are localized in the supercell. This gives hints on the location of the Wannier centers for the trial states.

The trial functions are considered as follows. Following the procedure mentioned in Ref. [126], we can expect the sites close to the π fluxes to be the most probable regions for Majorana wave functions. We confirm this by plotting the probability amplitude of each Majorana sublattice of the full supercell Hamiltonian:

$$\chi_{p,i}(\mathbf{k}) = \sum_{a=\pm}|\Gamma_{p,a,i}(\mathbf{k})|^2. \quad \text{(C2)}$$

This signifies the occupation probability of the targeted bands for each sublattice index, α for a $\mathbf{k}$ point. The highest probability indeed coincides at sites close to the π fluxes, as shown in Fig. 7. Based on this, we construct the trial functions for the $\boldsymbol{\alpha}$-Wannier Majorana orbital,

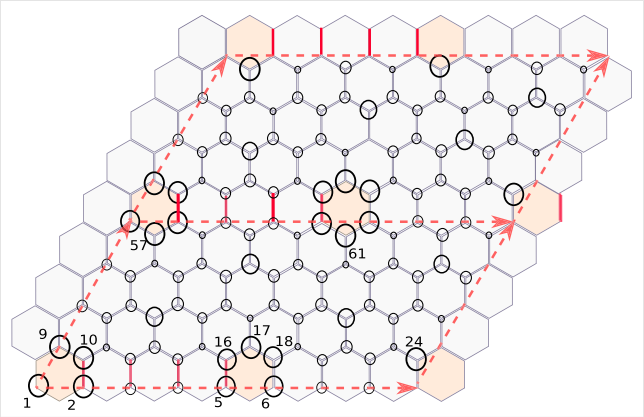


FIG. 7. We plot the orbital weight of the two lowest-energy ($p = 1$) particle-hole states $\sum_{\mathbf{k}} \chi_{p,i}(\mathbf{k})$ at different sites i, defined in Eq. (C2). The results are shown for the 4×4 flux configuration. The size of the open circles denotes the orbital weight strength. We note that the weight is largest around the π fluxes.

$$|\alpha, \pm, \mathbf{R}\rangle_t = \frac{1}{\sqrt{2N}} \sum_i^{2N} \delta(\mathbf{r} - \mathbf{R} - \mathbf{t}_i)|\mathbf{r}\rangle, \tag{C3}$$

where $\mathbf{t}_i$ are the positions of the original Majorana sublattices in the full Hamiltonian within the $\mathbf{R}$ supercell. For example, for the 4×4 configuration are shown in Fig. 7, the sublattice indices for the trial function are with $(\alpha, +) \in \{1, 9, 10\}$ and $(\alpha, -) \in \{5, 16, 17, 18\}$. There is no unique definition for these trial functions. The good choice is the functions that give 10%–20% change in the spread function, from the initial spread function to the final spreads after the minimization procedure. In the $\mathbf{k}$ space, we obtained $|\alpha, \pm, \mathbf{k}\rangle_t$ by the Fourier transformation given in Eq. (5). With these trial functions, the Wannier centers are shown in Fig. 4(a) for 4×4 configurations. In Fig. 4(b), we plot the dispersions of Majorana fermions from Wannierized orbitals, and it fits exact diagonalization (ED) results well with distances $\mathbf{R} \leq |9\mathbf{a}_1 + 9\mathbf{a}_2|$.

4. Values of tight-binding parameters

$$\mathcal{T}_{\mathbf{R},\mathbf{R}} = i\begin{pmatrix} 0 & -0.036 \\ 0.036 & 0 \end{pmatrix},$$

$$\mathcal{T}_{\mathbf{R},\mathbf{R}^{(1)}=(1,0)} = i\begin{pmatrix} 0.000 & 0.005 \\ -0.023 & -0.000 \end{pmatrix} = \mathcal{T}^{\dagger}_{\mathbf{R},-\mathbf{R}^{(1)}},$$

$$\mathcal{T}_{\mathbf{R},\mathbf{R}^{(2)}=(0,1)} = i\begin{pmatrix} 0.028 & -0.05 \\ -0.05 & -0.028 \end{pmatrix} = \mathcal{T}^{\dagger}_{\mathbf{R},-\mathbf{R}^{(2)}},$$

$$\mathcal{T}_{\mathbf{R},\mathbf{R}^{(3)}=(1,1)} = i\begin{pmatrix} -0.004 & 0.005 \\ -0.008 & -0.004 \end{pmatrix} = \mathcal{T}^{\dagger}_{\mathbf{R},-\mathbf{R}^{(3)}},$$

$$\mathcal{T}_{\mathbf{R},\mathbf{R}^{(4)}=(1,-1)} = i\begin{pmatrix} 0.018 & -0.008 \\ -0.038 & -0.018 \end{pmatrix} = \mathcal{T}^{\dagger}_{\mathbf{R},-\mathbf{R}^{(4)}},$$

$$\mathcal{T}_{\mathbf{R},\mathbf{R}^{(5)}=(2,0)} = i\begin{pmatrix} 0.025 & -0.002 \\ 0.012 & -0.25 \end{pmatrix} = \mathcal{T}^{\dagger}_{\mathbf{R},-\mathbf{R}^{(5)}},$$

$$\mathcal{T}_{\mathbf{R},\mathbf{R}^{(6)}=(0,2)} = i\begin{pmatrix} 0.005 & 0.006 \\ -0.029 & 0.005 \end{pmatrix} = \mathcal{T}^{\dagger}_{\mathbf{R},-\mathbf{R}^{(6)}},$$

$$\mathcal{T}_{\mathbf{R},\mathbf{R}^{(7)}=(1,2)} = i\begin{pmatrix} 0.003 & -0.002 \\ 0.011 & -0.003 \end{pmatrix} = -\mathcal{T}_{\mathbf{R},-\mathbf{R}^{(7)}},$$

$$\mathcal{T}_{\mathbf{R},\mathbf{R}^{(8)}=(1,-2)} = i\begin{pmatrix} -0.011 & -0.004 \\ -0.014 & 0.011 \end{pmatrix} = -\mathcal{T}_{\mathbf{R},-\mathbf{R}^{(8)}},$$

$$\mathcal{T}_{\mathbf{R},\mathbf{R}^{(9)}=(2,-1)} = i\begin{pmatrix} -0.006 & 0.003 \\ -0.026 & 0.006 \end{pmatrix} = \mathcal{T}^{\dagger}_{\mathbf{R},-\mathbf{R}^{(9)}},$$

$$\mathcal{T}_{\mathbf{R},\mathbf{R}^{(10)}=(2,1)} = i\begin{pmatrix} 0.001 & -0.001 \\ 0.001 & -0.001 \end{pmatrix} = \mathcal{T}^{\dagger}_{\mathbf{R},-\mathbf{R}^{(10)}},$$

$$\mathcal{T}_{\mathbf{R},\mathbf{R}^{(11)}=(2,2)} = i\begin{pmatrix} -0.017 & 0.001 \\ -0.004 & 0.017 \end{pmatrix} = \mathcal{T}^{\dagger}_{\mathbf{R},-\mathbf{R}^{(11)}},$$

$$\mathcal{T}_{\mathbf{R},\mathbf{R}^{(12)}=(2,-2)} = i\begin{pmatrix} 0.003 & 0.001 \\ 0.025 & -0.003 \end{pmatrix} = \mathcal{T}^{\dagger}_{\mathbf{R},-\mathbf{R}^{(12)}},$$

$$\mathcal{T}_{\mathbf{R},\mathbf{R}^{(13)}=(2,3)} = i\begin{pmatrix} 0.00 & 0.000 \\ 0.002 & 0.00 \end{pmatrix} = \mathcal{T}^{\dagger}_{\mathbf{R},-\mathbf{R}^{(13)}},$$

$$\mathcal{T}_{\mathbf{R},\mathbf{R}^{(14)}=(2,-3)} = i\begin{pmatrix} 0.003 & -0.003 \\ -0.010 & -0.003 \end{pmatrix} = \mathcal{T}^{\dagger}_{\mathbf{R},-\mathbf{R}^{(14)}},$$

$$\mathcal{T}_{\mathbf{R},\mathbf{R}^{(15)}=(1,3)} = i\begin{pmatrix} 0.000 & 0.00 \\ -0.004 & 0.00 \end{pmatrix} = \mathcal{T}^{\dagger}_{\mathbf{R},-\mathbf{R}^{(15)}},$$

$$\mathcal{T}_{\mathbf{R},\mathbf{R}^{(16)}=(1,-3)} = i\begin{pmatrix} -0.002 & 0.005 \\ 0.013 & 0.002 \end{pmatrix} = \mathcal{T}^{\dagger}_{\mathbf{R},-\mathbf{R}^{(16)}},$$

$$\mathcal{T}_{\mathbf{R},\mathbf{R}^{(17)}=(3,2)} = i\begin{pmatrix} 0.00 & 0.000 \\ 0.002 & 0.00 \end{pmatrix} = \mathcal{T}^{\dagger}_{\mathbf{R},-\mathbf{R}^{(17)}},$$

$$\mathcal{T}_{\mathbf{R},\mathbf{R}^{(18)}=(3,-2)} = i\begin{pmatrix} 0.00 & 0.000 \\ -0.006 & 0.00 \end{pmatrix} = \mathcal{T}^{\dagger}_{\mathbf{R},-\mathbf{R}^{(18)}},$$

$$\mathcal{T}_{\mathbf{R},\mathbf{R}^{(19)}=(3,3)} = i\begin{pmatrix} 0.000 & 0.000 \\ -0.001 & 0.000 \end{pmatrix} = \mathcal{T}^{\dagger}_{\mathbf{R},-\mathbf{R}^{(19)}},$$

$$\mathcal{T}_{\mathbf{R},\mathbf{R}^{(20)}=(3,-3)} = i\begin{pmatrix} -0.002 & 0.001 \\ -0.002 & 0.003 \end{pmatrix} = \mathcal{T}^{\dagger}_{\mathbf{R},-\mathbf{R}^{(20)}}. \tag{C4}$$

The lattice vectors are given above in terms of the Miller indices and $\mathbf{R} = (0, 0)$. The rest of the parameters are nearly zero and hence ignored in this table. The 2×2 matrices for each tensor component are in the two particle-hole Majorana basis of $a = \pm$.

[1] M. Greiter and F. Wilczek, *Fractional statistics*, Annu. Rev. Condens. Matter Phys. **15**, 131 (2024).

[2] R. Aguado and L. P. Kouwenhoven, *Majorana qubits for topological quantum computing*, Phys. Today **73**, No. 6, 44 (2020).

[3] B. Keimer and J. E. Moore, *The physics of quantum materials*, Nat. Phys. **13**, 1045 (2017).

[4] D. N. Basov, R. D. Averitt, and D. Hsieh, *Towards properties on demand in quantum materials*, Nat. Mater. **16**, 1077 (2017).

[5] Y. Tokura, M. Kawasaki, and N. Nagaosa, *Emergent functions of quantum materials*, Nat. Phys. **13**, 1056 (2017).

[6] D. Aasen, M. Hell, R. V. Mishmash, A. Higginbotham, J. Danon, M. Leijnse, T. S. Jespersen, J. A. Folk, C. M. Marcus, K. Flensberg, and J. Alicea, *Milestones toward Majorana-based quantum computing*, Phys. Rev. X **6**, 031016 (2016).

[7] S. D. Sarma, M. Freedman, and C. Nayak, *Majorana zero modes and topological quantum computation*, npj Quantum Inf. **1**, 15001 (2015).

[8] X.-G. Wen, *Quantum Field Theory of Many-Body Systems: From the Origin of Sound to an Origin of Light and Electrons* (Oxford University Press, New York, 2007).

[9] E. Fradkin, *Field Theories of Condensed Matter Physics*, 2nd ed. (Cambridge University Press, Cambridge, England, 2013).

[10] S. Sachdev, *Quantum Phase Transitions*, 2nd ed. (Cambridge University Press, Cambridge, England, 2011).

[11] *Semantic Techniques in Quantum Computation*, edited by S. Gay and I. Mackie (Cambridge University Press, Cambridge, England, 2009).

[12] C. W. J. Beenakker, *Random-matrix theory of Majorana fermions and topological superconductors*, Rev. Mod. Phys. **87**, 1037 (2015).

[13] A. Rahmani and M. Franz, *Interacting Majorana fermions*, Rep. Prog. Phys. **82**, 084501 (2019).

[14] S. C. Zhang, T. H. Hansson, and S. Kivelson, *Effective-field-theory model for the fractional quantum Hall effect*, Phys. Rev. Lett. **62**, 82 (1989).

[15] V. E. Tarasov, *Review of some promising fractional physical models*, Int. J. Mod. Phys. B **27**, 1330005 (2013).

[16] C. Chamon, *Quantum glassiness in strongly correlated clean systems: An example of topological overprotection*, Phys. Rev. Lett. **94**, 040402 (2005).

[17] A. Prem, J. Haah, and R. Nandkishore, *Glassy quantum dynamics in translation invariant fracton models*, Phys. Rev. B **95**, 155133 (2017).

[18] O. Hart, S. Gopalakrishnan, and C. Castelnovo, *Logarithmic entanglement growth from disorder-free localization in the two-leg compass ladder*, Phys. Rev. Lett. **126**, 227202 (2021).

[19] K. B. Yogendra, T. Das, and G. Baskaran, *Emergent glassiness in the disorder-free Kitaev model: Density matrix renormalization group study on a one-dimensional ladder setting*, Phys. Rev. B **108**, 165118 (2023).

[20] Y. Wan and N. P. Armitage, *Resolving continua of fractional excitations by spinon echo in THz 2D coherent spectroscopy*, Phys. Rev. Lett. **122**, 257401 (2019).

[21] R. M. Nandkishore, W. Choi, and Y. B. Kim, *Spectroscopic fingerprints of gapped quantum spin liquids, both conventional and fractonic*, Phys. Rev. Res. **3**, 013254 (2021).

[22] M. McGinley, M. Fava, and S. A. Parameswaran, *Signatures of fractional statistics in nonlinear pump-probe spectroscopy*, Phys. Rev. Lett. **132**, 066702 (2024).

[23] N. Marzari, A. A. Mostofi, J. R. Yates, I. Souza, and D. Vanderbilt, *Maximally localized Wannier functions: Theory and applications*, Rev. Mod. Phys. **84**, 1419 (2012).

[24] N. Marzari and D. Vanderbilt, *Maximally localized generalized Wannier functions for composite energy bands*, Phys. Rev. B **56**, 12847 (1997).

[25] I. Souza, N. Marzari, and D. Vanderbilt, *Maximally localized Wannier functions for entangled energy bands*, Phys. Rev. B **65**, 035109 (2001).

[26] D. J. Klein, *Degenerate perturbation theory*, J. Chem. Phys. **61**, 786 (1974).

[27] I. Shavitt and L. T. Redmon, *Quasidegenerate perturbation theories. A canonical van Vleck formalism and its relationship to other approaches*, J. Chem. Phys. **73**, 5711 (1980).

[28] C. Cohen-Tannoudji, B. Diu, and F. Laloë, *Quantum Mechanics*, A Wiley—Interscience Publication Vol. 1 (Wiley, New York, 1977).

[29] P. W. Anderson, G. Baskaran, Z. Zou, and T. Hsu, *Resonating–valence-bond theory of phase transitions and superconductivity in* La_2CuO_4*-based compounds*, Phys. Rev. Lett. **58**, 2790 (1987).

[30] P. Fazekas and P. W. Anderson, *On the ground state properties of the anisotropic triangular antiferromagnet*, Philos. Mag. **30**, 423 (1974).

[31] J. R. Schrieffer and P. A. Wolff, *Relation between the Anderson and Kondo Hamiltonians*, Phys. Rev. **149**, 491 (1966).

[32] S. Bravyi, D. P. DiVincenzo, and D. Loss, *Schrieffer–Wolff transformation for quantum many-body systems*, Ann. Phys. (Amsterdam) **326**, 2793 (2011).

[33] G. Giuliani and G. Vignale, *Quantum Theory of the Electron Liquid* (Cambridge University Press, Cambridge, England, 2005), Chap. 8.6.

[34] Y. Wu and X. Yang, *Strong-coupling theory of periodically driven two-level systems*, Phys. Rev. Lett. **98**, 013601 (2007).

[35] R. K. Nesbet, *Approximate methods in the quantum theory of many-fermion systems*, Rev. Mod. Phys. **33**, 28 (1961).

[36] R. L. Stratonovich, *On a method of calculating quantum distribution functions*, Sov. Phys. Dokl. **2**, 416 (1957).

[37] J. Hubbard, *Calculation of partition functions*, Phys. Rev. Lett. **3**, 77 (1959).

[38] A. Kitaev, *Fault-tolerant quantum computation by anyons*, Ann. Phys. (Amsterdam) **303**, 2 (2003).

[39] J. B. Kogut, *An introduction to lattice gauge theory and spin systems*, Rev. Mod. Phys. **51**, 659 (1979).

[40] T. B. Wahl, H.-H. Tu, N. Schuch, and J. I. Cirac, *Projected entangled-pair states can describe chiral topological states*, Phys. Rev. Lett. **111**, 236805 (2013).

[41] J. Haegeman, K. Van Acoleyen, N. Schuch, J. I. Cirac, and F. Verstraete, *Gauging quantum states: From global to*

local symmetries in many-body systems, Phys. Rev. X **5**, 011024 (2015).
[42] F. J. Wegner, *Duality in generalized Ising models and phase transitions without local order parameters*, J. Math. Phys. (N.Y.) **12**, 2259 (1971).
[43] A. Kitaev, *Anyons in an exactly solved model and beyond*, Ann. Phys. (Amsterdam) **321**, 2 (2006).
[44] G. Baskaran, S. Mandal, and R. Shankar, *Exact results for spin dynamics and fractionalization in the Kitaev model*, Phys. Rev. Lett. **98**, 247201 (2007).
[45] I. S. Tupitsyn, A. Kitaev, N. V. Prokof'ev, and P. C. E. Stamp, *Topological multicritical point in the phase diagram of the toric code model and three-dimensional lattice gauge Higgs model*, Phys. Rev. B **82**, 085114 (2010).
[46] Z.-C. Gu and X.-G. Wen, *Symmetry-protected topological orders for interacting fermions: Fermionic topological nonlinear σ models and a special group supercohomology theory*, Phys. Rev. B **90**, 115141 (2014).
[47] N. D. Patel and N. Trivedi, *Magnetic field-induced intermediate quantum spin liquid with a spinon Fermi surface*, Proc. Natl. Acad. Sci. U.S.A. **116**, 12199 (2019).
[48] M. Gohlke, R. Moessner, and F. Pollmann, *Dynamical and topological properties of the Kitaev model in a [111] magnetic field*, Phys. Rev. B **98**, 014418 (2018).
[49] Z. Zhu, I. Kimchi, D. N. Sheng, and L. Fu, *Robust non-Abelian spin liquid and a possible intermediate phase in the antiferromagnetic Kitaev model with magnetic field*, Phys. Rev. B **97**, 241110(R) (2018).
[50] H.-C. Jiang, C.-Y. Wang, B. Huang, and Y.-M. Lu, *Field induced quantum spin liquid with spinon Fermi surfaces in the Kitaev model*, arXiv:1809.08247.
[51] C. Hickey and S. Trebst, *Emergence of a field-driven U(1) spin liquid in the Kitaev honeycomb model*, Nat. Commun. **10**, 1 (2019).
[52] D. A. S. Kaib, S. M. Winter, and R. Valentí, *Kitaev honeycomb models in magnetic fields: Dynamical response and dual models*, Phys. Rev. B **100**, 144445 (2019).
[53] E. S. Sørensen, A. Catuneanu, J. S. Gordon, and H.-Y. Kee, *Heart of entanglement: Chiral, nematic, and incommensurate phases in the Kitaev-gamma ladder in a field*, Phys. Rev. X **11**, 011013 (2021).
[54] V. Lahtinen, A. W. W. Ludwig, J. K. Pachos, and S. Trebst, *Topological liquid nucleation induced by vortex-vortex interactions in Kitaev's honeycomb model*, Phys. Rev. B **86**, 075115 (2012).
[55] V. Lahtinen, A. W. W. Ludwig, and S. Trebst, *Perturbed vortex lattices and the stability of nucleated topological phases*, Phys. Rev. B **89**, 085121 (2014).
[56] S.-S. Zhang, Z. Wang, G. B. Halász, and C. D. Batista, *Vison crystals in an extended Kitaev model on the honeycomb lattice*, Phys. Rev. Lett. **123**, 057201 (2019).
[57] S.-S. Zhang, C. D. Batista, and G. B. Halász, *Toward Kitaev's sixteenfold way in a honeycomb lattice model*, Phys. Rev. Res. **2**, 023334 (2020).
[58] R. R. Biswas, *Majorana fermions in vortex lattices*, Phys. Rev. Lett. **111**, 136401 (2013).
[59] J. Nasu, J. Yoshitake, and Y. Motome, *Thermal transport in the Kitaev model*, Phys. Rev. Lett. **119**, 127204 (2017).
[60] J.-N. Fuchs, S. Patil, and J. Vidal, *Parity of Chern numbers in the Kitaev honeycomb model and the sixteenfold way*, Phys. Rev. B **102**, 115130 (2020).
[61] A. Koga, Y. Murakami, and J. Nasu, *Majorana correlations in the Kitaev model with ordered-flux structures*, Phys. Rev. B **103**, 214421 (2021).
[62] S. Chulliparambil, L. Janssen, M. Vojta, H.-H. Tu, and U. F. P. Seifert, *Flux crystals, Majorana metals, and flat bands in exactly solvable spin-orbital liquids*, Phys. Rev. B **103**, 075144 (2021).
[63] A. Hashimoto, Y. Murakami, and A. Koga, *Majorana gap formation in the anisotropic Kitaev model with ordered flux configuration*, Phys. Rev. B **107**, 174428 (2023).
[64] D. J. Alspaugh, J.-N. Fuchs, A. Ritz-Zwilling, and J. Vidal, *Effective models for dense vortex lattices in the Kitaev honeycomb model*, Phys. Rev. B **109**, 115107 (2024).
[65] P. J. Ledwith, A. Vishwanath, and D. E. Parker, *Vortexability: A unifying criterion for ideal fractional Chern insulators*, Phys. Rev. B **108**, 205144 (2023).
[66] D. Otten, A. Roy, and F. Hassler, *Dynamical structure factor in the non-Abelian phase of the Kitaev honeycomb model in the presence of quenched disorder*, Phys. Rev. B **99**, 035137 (2019).
[67] K. Feng, N. B. Perkins, and F. J. Burnell, *Further insights into the thermodynamics of the Kitaev honeycomb model*, Phys. Rev. B **102**, 224402 (2020).
[68] A. Metavitsiadis and W. Brenig, *Flux mobility delocalization in the Kitaev spin ladder*, Phys. Rev. B **103**, 195102 (2021).
[69] G.-Y. Zhu and M. Heyl, *Subdiffusive dynamics and critical quantum correlations in a disorder-free localized Kitaev honeycomb model out of equilibrium*, Phys. Rev. Res. **3**, L032069 (2021).
[70] W.-H. Kao, J. Knolle, G. B. Halász, R. Moessner, and N. B. Perkins, *Vacancy-induced low-energy density of states in the Kitaev spin liquid*, Phys. Rev. X **11**, 011034 (2021).
[71] W.-H. Kao and N. B. Perkins, *Disorder upon disorder: Localization effects in the Kitaev spin liquid*, Ann. Phys. (Amsterdam) **435**, 168506 (2021).
[72] R. G. Pereira and R. Egger, *Electrical access to Ising anyons in Kitaev spin liquids*, Phys. Rev. Lett. **125**, 227202 (2020).
[73] M. Udagawa, S. Takayoshi, and T. Oka, *Scanning tunneling microscopy as a single Majorana detector of Kitaev's chiral spin liquid*, Phys. Rev. Lett. **126**, 127201 (2021).
[74] J. Kang and O. Vafek, *Symmetry, maximally localized Wannier states, and a low-energy model for twisted bilayer graphene narrow bands*, Phys. Rev. X **8**, 031088 (2018).
[75] S. Peotta and P. Törmä, *Superfluidity in topologically nontrivial flat bands*, Nat. Commun. **6**, 8944 (2015).
[76] J. Herzog-Arbeitman, V. Peri, F. Schindler, S. D. Huber, and B. A. Bernevig, *Superfluid weight bounds from symmetry and quantum geometry in flat bands*, Phys. Rev. Lett. **128**, 087002 (2022).
[77] L. Zou, H. C. Po, A. Vishwanath, and T. Senthil, *Band structure of twisted bilayer graphene: Emergent symmetries, commensurate approximants, and Wannier obstructions*, Phys. Rev. B **98**, 085435 (2018).

[78] A. Kruchkov, *Quantum geometry, flat Chern bands, and Wannier orbital quantization*, Phys. Rev. B **105**, L241102 (2022).

[79] M. Koshino, N. F. Q. Yuan, T. Koretsune, M. Ochi, K. Kuroki, and L. Fu, *Maximally localized Wannier orbitals and the extended Hubbard model for twisted bilayer graphene*, Phys. Rev. X **8**, 031087 (2018).

[80] F. Schindler, B. Bradlyn, M. H. Fischer, and T. Neupert, *Pairing obstructions in topological superconductors*, Phys. Rev. Lett. **124**, 247001 (2020).

[81] We make an approximation that the single-particle dispersion, many-body interaction, and superconducting order parameters are short-ranged, restricting to a few nearest neighbors only. (This truncation of the Fourier series to a polynomial of few sites gives a finite width of the single-particle states in both position and momentum space, and the number of nearest neighbors $\mathcal{N}$ to be considered is determined within a numerical procedure by fitting to the band structure at all $\mathbf{k}$ points. This yields the so-called compact localized orbitals for the flat band in the Wannierization procedure).

[82] Note that in our procedure it is easy to implement the lattice (point or space) group symmetry by doing the invariant rotation on the Bloch phase spinor $\mathbf{Z}_n(\mathbf{k})$.

[83] J.-W. Rhim and B.-J. Yang, *Classification of flat bands according to the band-crossing singularity of Bloch wave functions*, Phys. Rev. B **99**, 045107 (2019).

[84] S. M. Zhang and L. Jin, *Compact localized states and localization dynamics in the dice lattice*, Phys. Rev. B **102**, 054301 (2020).

[85] Y. Onishi and L. Fu, *Fundamental bound on topological gap*, Phys. Rev. X **14**, 011052 (2024).

[86] A. Bouhon, A. Timmel, and R.-J. Slager, *Quantum geometry beyond projective single bands*, arXiv:2303.02180.

[87] T. Das, *Weyl semimetal and superconductor designed in an orbital-selective superlattice*, Phys. Rev. B **88**, 035444 (2013).

[88] The higher-energy bands also carry finite Chern numbers, resulting in a total Chern number of $C = \pm 2$ for the filled and empty bands, consistent with Ref. [60]. However, for the construction of the effective lattice model, we focus exclusively on the two low-energy bands with $C = \pm 1$.

[89] A. A. Mostofi, J. R. Yates, G. Pizzi, Y.-S. Lee, I. Souza, D. Vanderbilt, and N. Marzari, *An updated version of WANNIER90: A tool for obtaining maximally-localised Wannier functions*, Comput. Phys. Commun. **185**, 2309 (2014).

[90] C. Harada, A. Ono, and J. Nasu, *Field-driven spatiotemporal manipulation of Majorana zero modes in a Kitaev spin liquid*, Phys. Rev. B **108**, L241118 (2023).

[91] D. J. Thouless, M. Kohmoto, M. P. Nightingale, and M. den Nijs, *Quantized Hall conductance in a two-dimensional periodic potential*, Phys. Rev. Lett. **49**, 405 (1982).

[92] The symmetric tensor $\eta_{\mu\nu}$ for the hexagonal lattice becomes $\eta_{\mu\nu} = \hat{\mathbf{G}}_\mu . \hat{\mathbf{G}}_\nu = \left(\begin{smallmatrix} 1 & -1/2 \\ -1/2 & 1 \end{smallmatrix}\right)$.

[93] A. Kitaev and J. Preskill, *Topological entanglement entropy*, Phys. Rev. Lett. **96**, 110404 (2006).

[94] M. Levin and X.-G. Wen, *Detecting topological order in a ground state wave function*, Phys. Rev. Lett. **96**, 110405 (2006).

[95] R. Nehra, D. S. Bhakuni, A. Ramachandran, and A. Sharma, *Flat bands and entanglement in the Kitaev ladder*, Phys. Rev. Res. **2**, 013175 (2020).

[96] Y. Kuno, *Extended flat band, entanglement, and topological properties in a Creutz ladder*, Phys. Rev. B **101**, 184112 (2020).

[97] C. Brouder, G. Panati, M. Calandra, C. Mourougane, and N. Marzari, *Exponential localization of Wannier functions in insulators*, Phys. Rev. Lett. **98**, 046402 (2007).

[98] D. Monaco, G. Panati, A. Pisante, and S. Teufel, *Optimal decay of Wannier functions in Chern and quantum Hall insulators*, Commun. Math. Phys. **359**, 61 (2018).

[99] S. Peotta and P. Törmä, *Superfluidity in topologically nontrivial flat bands*, Nat. Commun. **6**, 8944 (2015).

[100] P. Törmä, S. Peotta, and B. A. Bernevig, *Superconductivity, superfluidity and quantum geometry in twisted multilayer systems*, Nat. Rev. Phys. **4**, 528 (2022).

[101] T. Neupert, L. Santos, C. Chamon, and C. Mudry, *Fractional quantum Hall states at zero magnetic field*, Phys. Rev. Lett. **106**, 236804 (2011).

[102] E. Tang, J.-W. Mei, and X.-G. Wen, *High-temperature fractional quantum Hall states*, Phys. Rev. Lett. **106**, 236802 (2011).

[103] K. Sun, Z. Gu, H. Katsura, and S. Das Sarma, *Nearly flatbands with nontrivial topology*, Phys. Rev. Lett. **106**, 236803 (2011).

[104] T. Neupert, C. Chamon, T. Iadecola, L. H. Santos, and C. Mudry, *Fractional (Chern and topological) insulators*, Phys. Scr. **2015**, 014005 (2015).

[105] N. Regnault and B. A. Bernevig, *Fractional Chern insulator*, Phys. Rev. X **1**, 021014 (2011).

[106] Z. Liu, E. J. Bergholtz, H. Fan, and A. M. Läuchli, *Fractional Chern insulators in topological flat bands with higher Chern number*, Phys. Rev. Lett. **109**, 186805 (2012).

[107] S. A. Parameswaran, R. Roy, and S. L. Sondhi, *Fractional quantum Hall physics in topological flat bands*, C.R. Phys. **14**, 816 (2013).

[108] M. Barkeshli, N. Y. Yao, and C. R. Laumann, *Continuous preparation of a fractional Chern insulator*, Phys. Rev. Lett. **115**, 026802 (2015).

[109] G. Möller and N. R. Cooper, *Fractional Chern insulators in Harper-Hofstadter bands with higher Chern number*, Phys. Rev. Lett. **115**, 126401 (2015).

[110] J. Behrmann, Z. Liu, and E. J. Bergholtz, *Model fractional Chern insulators*, Phys. Rev. Lett. **116**, 216802 (2016).

[111] C. H. Lee, M. Claassen, and R. Thomale, *Band structure engineering of ideal fractional Chern insulators*, Phys. Rev. B **96**, 165150 (2017).

[112] Z. Liu and E. J. Bergholtz, *Recent developments in fractional Chern insulators*, in Encyclopedia of Condensed Matter Physics, 2nd ed., edited by T. Chakraborty (Academic Press, Oxford, 2024), pp. 515–538.

[113] G. K. Gupta and T. Das, *Quantum spin Hall density wave insulator of correlated fermions*, Phys. Rev. B **95**, 161109 (R) (2017).

[114] R. Roy, *Band geometry of fractional topological insulators*, Phys. Rev. B **90**, 165139 (2014).

[115] S. H. Simon and M. S. Rudner, *Contrasting lattice geometry dependent versus independent quantities:*

Ramifications for Berry curvature, energy gaps, and dynamics, Phys. Rev. B **102**, 165148 (2020).
[116] S. Elitzur, *Impossibility of spontaneously breaking local symmetries*, Phys. Rev. D **12**, 3978 (1975).
[117] X.-G. Wen, *Quantum orders and symmetric spin liquids*, Phys. Rev. B **65**, 165113 (2002).
[118] F. Wang and A. Vishwanath, *Spin-liquid states on the triangular and kagomé lattices: A projective-symmetry-group analysis of Schwinger Boson states*, Phys. Rev. B **74**, 174423 (2006).
[119] X.-Y. Song, C. Wang, A. Vishwanath, and Y.-C. He, *Unifying description of competing orders in two-dimensional quantum magnets*, Nat. Commun. **10**, 4254 (2019).
[120] S.-H. Jang, Y. Kato, and Y. Motome, *Vortex creation and control in the Kitaev spin liquid by local bond modulations*, Phys. Rev. B **104**, 085142 (2021).
[121] X. Wang, M. Laav, I. Volotsenko, A. Frydman, and B. Kalisky, *Visualizing current in superconducting networks*, Phys. Rev. Appl. **17**, 024073 (2022).
[122] T. Senthil, A. Vishwanath, L. Balents, S. Sachdev, and M. P. A. Fisher, *Deconfined quantum critical points*, Science **303**, 1490 (2004).
[123] T. Senthil, *Deconfined quantum critical points: A review*, arXiv:2306.12638.
[124] M. Kohmoto, *Topological invariant and the quantization of the Hall conductance*, Ann. Phys. (N.Y.) **160**, 343 (1985).
[125] T. Thonhauser and D. Vanderbilt, *Insulator/Chern-insulator transition in the Haldane model*, Phys. Rev. B **74**, 235111 (2006).
[126] A. A. Soluyanov and D. Vanderbilt, *Wannier representation of F_2 topological insulators*, Phys. Rev. B **83**, 035108 (2011).
[127] R. Yu, X. L. Qi, A. Bernevig, Z. Fang, and X. Dai, *Equivalent expression of F_2 topological invariant for band insulators using the non-Abelian Berry connection*, Phys. Rev. B **84**, 075119 (2011).
[128] X.-L. Qi, *Generic wave-function description of fractional quantum anomalous Hall states and fractional topological insulators*, Phys. Rev. Lett. **107**, 126803 (2011).
[129] T. M. Gunawardana, A. M. Turner, and R. Barnett, *Optimally localized single-band Wannier functions for two-dimensional Chern insulators*, Phys. Rev. Res. **6**, 023046 (2024).
[130] F. Xie, Y. Fang, L. Chen, J. Cano, and Q. Si, *Chern bands' optimally localized Wannier functions and fractional Chern insulators*, arXiv:2407.08920.
[131] H. Wang, R. Shi, Z. Liu, and J. Wang, *Orbital description of Landau levels*, arXiv:2411.13071.
[132] G. Strinati, *Multipole wave functions for photoelectrons in crystals. III. The role of singular points in the band structure and the tails of the Wannier functions*, Phys. Rev. B **18**, 4104 (1978).
[133] D. L. Bergman, C. Wu, and L. Balents, *Band touching from real-space topology in frustrated hopping models*, Phys. Rev. B **78**, 125104 (2008).
[134] J. Herzog-Arbeitman, V. Peri, F. Schindler, S. D. Huber, and B. A. Bernevig, *Superfluid weight bounds from symmetry and quantum geometry in flat bands*, Phys. Rev. Lett. **128**, 087002 (2022).
[135] S. Flach, D. Leykam, J. D. Bodyfelt, P. Matthies, and A. S. Desyatnikov, *Detangling flat bands into Fano lattices*, Europhys. Lett. **105**, 30001 (2014).
[136] J. Dubail and N. Read, *Tensor network trial states for chiral topological phases in two dimensions and a no-go theorem in any dimension*, Phys. Rev. B **92**, 205307 (2015).
[137] L. Morales-Inostroza and R. A. Vicencio, *Simple method to construct flat-band lattices*, Phys. Rev. A **94**, 043831 (2016).
[138] W. Maimaiti, A. Andreanov, H. C. Park, O. Gendelman, and S. Flach, *Compact localized states and flat-band generators in one dimension*, Phys. Rev. B **95**, 115135 (2017).
[139] N. Read, *Compactly supported Wannier functions and algebraic k-theory*, Phys. Rev. B **95**, 115309 (2017).
[140] S. M. Zhang and L. Jin, *Compact localized states and localization dynamics in the dice lattice*, Phys. Rev. B **102**, 054301 (2020).
[141] B. Bradlyn, L. Elcoro, J. Cano, M. G. Vergniory, Z. Wang, C. Felser, M. I. Aroyo, and B. A. Bernevig, *Topological quantum chemistry*, Nature (London) **547**, 298 (2017).
[142] H. C. Po, A. Vishwanath, and H. Watanabe, *Symmetry-based indicators of band topology in the 230 space groups*, Nat. Commun. **8** (2017).
[143] F. Schindler and B. A. Bernevig, *Noncompact atomic insulators*, Phys. Rev. B **104**, L201114 (2021).
[144] Y.-C. Chen, Y.-P. Lin, and Y.-J. Kao, *Stably protected gapless edge states without Wannier obstruction*, Phys. Rev. B **107**, 075126 (2023).